The Astronomical Journal, 145:101 (22pp), 2013 April doi:10.1088/0004-6256/145/4/101

UPDATED NEARBY GALAXY CATALOG

Igor D. Karachentsev, Dmitry I. Makarov, and Elena I. Kaisina
Special Astrophysical Observatory RAS, Nizhnij Arkhyz, Karachai-Cherkessian Republic, 369167, Russia; ikar@sao.ru
Received 2012 November 16; accepted 2013 January 11; published 2013 March 12

ABSTRACT

We present an all-sky catalog of 869 nearby galaxies having individual distance estimates within 11 Mpc or corrected radial velocities $V_{LG} < 600$ km s^{-1}. The catalog is a renewed and expanded version of the Catalog of Neighboring Galaxies by Karachentsev et al. It collects data on the following galaxy observables: angular diameters, apparent magnitudes in far-UV, B, and K_s bands, Hα and H I fluxes, morphological types, H I-line widths, radial velocities, and distance estimates. In this Local Volume (LV) sample, 108 dwarf galaxies still remain without measured radial velocities. The catalog yields also calculated global galaxy parameters: linear Holmberg diameter, absolute B magnitude, surface brightness, H I mass, stellar mass estimated via K-band luminosity, H I rotational velocity corrected for galaxy inclination, indicative mass within the Holmberg radius, and three kinds of "tidal index," which quantify the local density environment. The catalog is supplemented with data based on the local galaxies, which presents their optical and available Hα images, as well as other services. We briefly discuss the Hubble flow within the LV and different scaling relations that characterize galaxy structure and global star formation in them. We also trace the behavior of the mean stellar mass density, H I-mass density, and star formation rate density within the volume considered.

Key words: galaxies: distances and redshifts – galaxies: fundamental parameters

Online-only material: color figures, machine-readable and VO tables

1. INTRODUCTION

As previously noted by Peebles (1993), Peebles & Nusser (2010), and Peebles et al. (2001), the study of a representative sample of the nearest galaxies is a source of important data on the formation and evolution of large-scale structure of the universe. Numerous N-body simulations widely applied today in various cosmological models suggest observational verification of their results via comparing the properties of galaxies in a reference volume of fixed size. However, almost all existing galaxy catalogs limit the samples, by galaxy flux (apparent magnitude) but not distance. Because galaxies differ by a large range of luminosities and surface brightnesses, the creation of a sample limited by a fixed volume has proved extremely difficult. As an example, note that the famous Revised Shapley–Ames Catalog (Sandage & Tammann 1981) contains the 1246 brightest galaxies ($B_T < 13^m.2$) across the sky, but only about 100 of them, i.e., 8%, make it into the sample of the most nearby galaxies with distances from us within 10 Mpc.

The study of galaxies in the Local Volume (LV), conditionally limited by a radius of $D = 10$ Mpc, has an obvious advantage, since many dwarf galaxies, otherwise inaccessible for observations at large distances, were discovered in it. These "test particles" with measured radial velocities and distances trace the Hubble flow with unprecedentedly high detail. For a comparison note that in the most extensive Sloan Digital Sky Survey (SDSS; Abazajian et al. 2009) the average distance between galaxies with known radial velocities is about 8 Mpc, whereas in the LV ($D < 10$ Mpc) the number of galaxies with measured velocities is greater than 630.

Until the late 1990s the development of observational cosmology in the local universe was hampered by the scarcity of data on the distances of even the most nearby galaxies, located just outside the Local Group boundaries. The deployment of the unique capabilities of the *Hubble Space Telescope* (*HST*) combined with a new method for determining distances to galaxies by the luminosity of the tip of their red giant branch (TRGB; Lee et al. 1993) made it possible to carry out mass distance measurements of more than 250 nearby galaxies with an accuracy of 5%–10%. The summary of data on distances, radial velocities, and other parameters of galaxies in the LV ($D \leqslant 10$ Mpc) was presented in the Catalog of Neighboring Galaxies (CNG; Karachentsev et al. 2004). This volume contains dwarf galaxies with luminosities 10^4 times lower than that of the Milky Way, and it includes more than a dozen groups similar to our Local Group in size and population. A detailed pattern of the motions of and around the galaxies in these groups has for the first time revealed some unexpected features in the Hubble flow at scales of 1–3 Mpc. New evidence has appeared that the Hubble velocity–distance diagrams around the Local Group and other neighboring groups are characterized by a small dispersion of peculiar velocities ~30 km s^{-1} (Karachentsev et al. 2009). The Local Group overdensity decelerates the surrounding galaxies, which leads to curving the local Hubble flow. This effect can be observed because of the small chaotic motions as well as the minor distance measurement errors of nearby galaxies. The achieved distance accuracy allows us to determine the total mass of nearby groups with a relative error of ~30% by the value of radius of the "zero-velocity sphere" R_0, which separates the group volume from the remaining expanding neighborhood (Karachentsev et al. 2009; Karachentsev 2005).

It should be emphasized that the "R_0" method provides an estimate of the group mass independent of the virial theorem, and this total mass estimate refers to a scale 3.5–4.0 times larger than the virial radius of the group. It is noteworthy that the agreement of mass estimates of nearby groups based on the external and internal (virial) motions of galaxies is achieved only in the presence of the cosmological parameter $\Omega_\lambda \simeq 0.7$. This means that the observed properties of the Local Hubble flow give direct and independent evidence of the presence in the universe of a specific medium, dark energy, discovered from observations of distant supernovae.

As shown by Dalcanton et al. (2009), Weisz et al. (2011), and other authors, the deep color–magnitude diagrams obtained at the *HST* for the stellar population of nearby galaxies provide an opportunity to reconstruct the history of star formation in them with a resolution of ∼(0.1–1) Gyr. This approach is an important observational tool for modeling the evolution of galaxies in different environments.

The creation of a representative sample of galaxies in the LV originates from a list of 179 galaxies compiled by Kraan-Korteweg & Tammann (1979), which contains galaxies with radial velocities $V_{\rm LG} < 500$ km s^{-1} relative to the Local Group centroid, except for members of the nearby Virgo cluster. Later, Karachentsev (1994) and Karachentsev et al. (1999) increased the number of galaxies in the LV to 226 and 303 objects, respectively. In 1998–2001 Karachentseva and her colleagues undertook a systematic search for new nearby dwarf galaxies using the POSS-II/ESO/SERC photographic sky survey. These efforts (Karachentseva & Karachentsev 1998, 2000; Karachentseva et al. 1999). Along with the subsequent survey of new objects in the H I line of neutral hydrogen (Huchtmeier et al. 2000, 2001, 2003) have considerably enriched the sample of galaxies in the LV. A significant number of new irregular dwarf galaxies with radial velocities $V_{\rm LG} < 500$ km s^{-1} were observed within the "blind" H I survey of the southern sky performed at the Parkes radio telescope (Staveley-Smith et al. 1998; Kilborn et al. 2002; Zwaan et al. 2003; Koribalski et al. 2004; Meyer et al. 2004). The summary of these data, increasing the number of galaxies in the LV up to $N = 450$, is reflected in the CNG catalog (Karachentsev et al. 2004).

In subsequent years, the growth of the LV sample occurred via the detection of new dwarf galaxies within the SDSS optical sky survey (Abazajian et al. 2009), the H I Parkes All Sky Survey (HIPASS; Wong et al. 2006), Arecibo Legacy Fast ALFA Survey (ALFALFA; Giovanelli et al. 2005; Haynes et al. 2011), and Westerbork (Kovaĉ et al. 2009) H I surveys of the northern sky, and as a result of the systematic search for dwarf satellites of extremely low luminosity, resolved into stars, around the Milky Way (Willman et al. 2005; Belokurov et al. 2006), M 31 (Ibata et al. 2007; Martin et al. 2009), and M 81 (Chiboucas et al. 2009). By now the number of candidate members in the LV with distances $D \leqslant 10$ Mpc has reached 720. It is clear that massive optical sky surveys such as the Pan-STARRS (Tonry et al. 2012) and deeper "blind" H I surveys of the northern and southern sky will increase this number up to and more than 1000.

2. THE LOCAL VOLUME SAMPLE CRITERION

The selection of galaxies in the local spherical volume of 10 Mpc radius by the condition $V_{\rm LG} \leqslant 500$ km s^{-1}, used by Kraan-Korteweg & Tammann (1979), assumed the Hubble parameter value of $H_0 = 50$ km s^{-1} Mpc^{-1}. At the current value of $H_0 = 73$ km s^{-1} Mpc^{-1} (Spergel et al. 2007), the limit set for radial velocities should be raised to $V_{\rm LG} \leqslant 730$ km s^{-1}. However, the radial velocity of a galaxy is only an approximate indication of its distance. In addition to the virial component of velocity inherent in the nearby group members, the local velocity field is also affected by the presence of a nearby, rich Virgo cluster at a distance of 16.5 Mpc with a velocity dispersion of $\sigma_v \simeq 650$ km s^{-1}, and an extensive Local Void (Tully 1988), which occupies about a quarter of the celestial sphere. According to Tully et al. (2008), the presence of these two main elements of the local large-scale structure generates two velocity components of the Local Group and surrounding galaxies: ∼180 km s^{-1} toward the Virgo cluster center ($12^{\rm h}30^{\rm m} + 12^\circ$) and ∼260 km s^{-1} in the direction away from the Local Void center, located in the region ∼($19^{\rm h}00^{\rm m}$+3°). An almost complete absence of galaxies in the region of the Local Void and their relative excess in the opposite direction creates a specific selection effect: most of the galaxies at a distance of $D = 10$ Mpc generally have radial velocities much lower than the expected value of ∼730 km s^{-1}.

There are recent indications that the filaments and walls of the large-scale structure may have collective motions with an amplitude of ∼500 km s^{-1}. Perhaps the closest example of such great non-virial motions is the Coma I region, where a "flock" of galaxies around NGC 4150 at a distance of $D \sim 15$ Mpc is moving toward us with a peculiar average velocity of −800 km s^{-1} (Karachentsev et al. 2011). To our regret, we have to state that the local field of peculiar velocities of galaxies is still poorly studied, and the proposed radial velocity correction schemes for coherent non-Hubble motions such as the model of pure Virgo-centric flow (Kraan-Korteweg 1986; Masters 2005) turn out to be too simplified. Therefore, a low radial velocity of the assumed nearby galaxy is not yet a reliable indicator of its proximity.

An ideal solution would be a direct measurement of distances to all nearby galaxy candidates using *HST*. As shown by Rizzi et al. (2007), the tip of the TRGB method gives a distance accuracy of ∼5% regardless of the galaxy morphological type. During the exposure time with Advanced Camera for Survey at *HST*, corresponding to one or two orbits, the TRGB method allows us to measure accurate distances up to 7–10 Mpc, i.e., to completely solve the problem of creating a fair sample of the LV. The cost of the method is, however, 1000–2000 orbits of *HST*.

Other methods of distance measurement may either be used for a small number of objects (the supernova method, the Cepheid method), or be applicable only to galaxies of fixed morphology (e.g., method of surface brightness fluctuations, Tully–Fisher and Faber–Jackson methods), or have an accuracy not better than 25% (method of brightest stars).

Given all these circumstances, we have included in the LV sample the galaxies having radial velocities with respect to centroid of the Local Group

$$V_{\rm LG} < 600\,{\rm km\,s^{-1}}, \quad (1)$$

or the galaxies with distance estimates

$$D < 11.0\,{\rm Mpc}. \quad (2)$$

A simultaneous fulfillment of both conditions (1) and (2) is not required. Here, we took into account the fact that some galaxies at distances ∼(7–10) Mpc may have orbital/virial velocities that place them in the region of $V_{\rm LG} > 600$ km s^{-1} on the Hubble diagram, while other galaxies, projected onto the Virgo cluster, are expected to have an additional positive velocity component due to their infall toward the cluster.

The velocity–distance diagram for 673 galaxies of the LV is presented in Figure 1. Beyond the upper edge of the figure, there are 16 galaxies with $D = (7–11)$ Mpc and $V_{\rm LG} > 1100$ km s^{-1}, almost all of them located near the line of sight, directed toward the Virgo cluster center. Beyond the right edge of the figure, 72 galaxies with $V_{\rm LG} < 600$ km s^{-1} are located, but with distance estimates over 11 Mpc. We did not exclude such objects from the sample for two reasons: (1) their distance estimates cannot quite be reliable and (2) the distribution of such galaxies on the

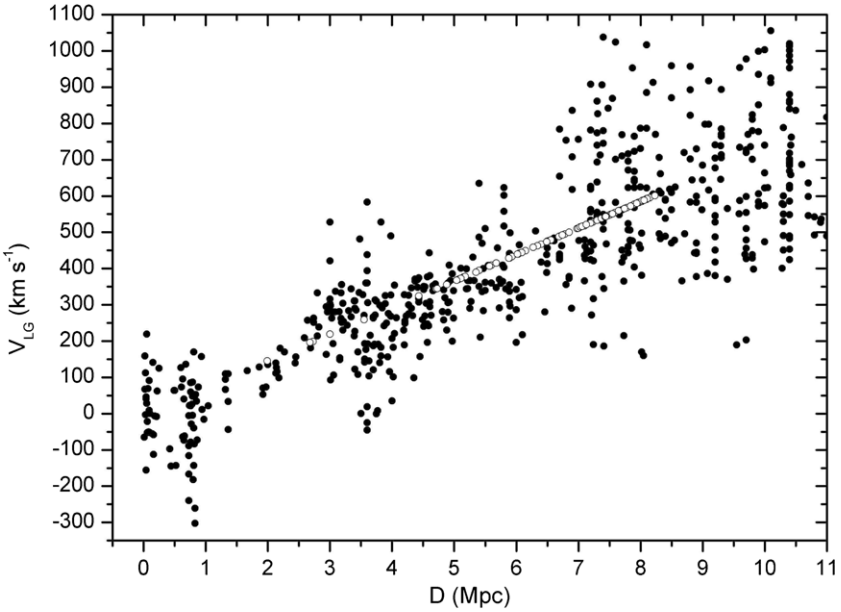

Figure 1. Hubble flow around the Local Group centroid. Some galaxies in the distance range 2–8 Mpc without individual distance estimates are drawn to trace the slope $H_0 = 73$ km s^{-1} Mpc^{-1} (open circles).

sky may outline coherent motions in nearby diffuse filaments. In addition, the list of objects in the LV contains 108 galaxies with individual distance estimates of $D < 10$ Mpc, which still have their radial velocities unmeasured.

Therefore, our total list of galaxies in the LV consists of 869 objects. As can be seen from Figure 1, about one-third of the galaxies located in the upper right corner could be considered to belong to the $D < 10$ Mpc volume only conditionally, since their typical distance measurement error is ∼2 Mpc. It also follows from these data that limiting the sample to condition (1) would only introduce a strong selective effect, distorting the kinematic pattern of the LV.

3. THE REPLENISHED CATALOG

Compiling the updated catalog of nearby galaxies, we generally followed the same sequence of presenting the observational data. Moreover, the catalog includes new parameters (Hα emission line fluxes, far-ultraviolet fluxes) that characterize the current star formation activity in galaxies. In addition to this catalog, we created an online database located at http://www.sao.ru/lv/lvgdb, which accumulates both observed and calculated integral parameters of the galaxies, presents galaxy images, and gives numerous references to the sources of the observables. The structure of the LV galaxy database is described by Kaisina et al. (2012). The list of 869 galaxies, included in the updated CNG catalog, is presented in Table 1. Its columns contain the following galaxy characteristics.

1. Name of the galaxy or its number in well-known catalogs. The LV database lists all alternative names/numbers, including the galaxy PGC number in the LEDA Extragalactic Database (Paturel et al. 2003).
2. Equatorial coordinates of the galaxy center for the epoch (J2000.0).
3. Major angular diameter in arcminutes, corresponding to the Holmberg isophote (∼$26^m.5$ arcsec^{-2}) in the B band. The a_{26} measurements were performed visually, but photometric profiles of different-type galaxies were used for their calibration based on the data by Bremnes et al. (1998, 1999, 2000) and Makarova et al. (2009). It should be noted that some dwarf galaxies of extremely low surface brightness (especially those resolved into individual stars) have a central surface brightness fainter than the Holmberg isophote. In these cases, the diameter a_{26} instead corresponds to the exponential scale h of their brightness profile.
4. Apparent axial ratio, measured at the Holmberg isophote.
5. Galactic extinction in the B band according to Schlegel et al. (1998).
6. Apparent magnitude of the galaxy in the far ultraviolet, $m_{\rm FUV}$, ($\lambda_{\rm eff}$ = 1539 Å, FWHM = 269 Å) according to data from the UV survey performed at the *Galaxy Evolution Explorer* (*GALEX*; Martin et al. 2005; Gil de Paz et al. 2007). For 295 galaxies the asymptotic $m_{\rm FUV}$ magnitudes were taken from Lee et al. (2011) and are presented in Table 3 without correction for Galactic extinction. For other galaxies, the *GALEX* data on the far-UV (FUV) fluxes and FUV magnitudes were extracted from the NASA Extragalactic Database (NED), summing fluxes from all structural knots within the optical galaxy image.
7. Apparent integral magnitude of the galaxy in the B band, the sources of which are listed in the LV database as well as in Table 3. If a galaxy lacks the photometric B_T, its apparent magnitude was estimated by eye, comparing with images of other galaxies of similar structure with measured B_T. In such cases, as a rule for objects of low surface brightness, a typical B_T error estimate amounts to ∼$0^m.5$.
8. Integral magnitude of galaxy in the Hα emission line as seen in the Cousins R band. Following the approach by Fukugita et al. (1995), we determined it to be

$$m_{\rm H\alpha} = -2.5\log(F_{\rm H\alpha}) - 13.64, \quad (3)$$

where $F_{\rm H\alpha}$ is the integral flux in the Hα line in units of erg cm^{-2} s^{-1}. The main source of the flux data is the Hα survey of the LV galaxies performed at the 6 m telescope of SAO RAS (Kaisin & Karachentsev 2006, 2008; Karachentsev & Kaisin 2007, 2010), as well as the survey by Kennicutt et al. (2008). References to Hα data on individual

Table 1
Catalog of Nearby Galaxies

Name	R.A. J2000.0 Decl.	a_{26}	b/a	A_B^G	$m_{\rm FUV}$	B_T	$m_{\rm H\alpha}$	K_s		m_{21}	W_{50}	T	$T_{\rm dw}$		V_h	D	Method
(1)	(2)	(3)	(4)	(5)	(6)	(7)	(8)	(9)		(10)	(11)	(12)	(13)	(14)	(15)	(16)	(17)
UGC 12894	000022.5+392944	1.02	0.87	0.47	17.57	16.80	19.91	14.02	*	15.66	34	10	Ir	L	335	8.47	TF
WLM	000158.1−152740	11.48	0.35	0.16	12.80	11.03	15.56	9.00		11.19	53	9	Im	N	−122	0.97	TRGB
And XVIII	000214.5+450520	1.40	0.99	0.45	>23.00	17.00		12.49	*			−3	Sph	L	−332	1.36	TRGB
ESO 409−015	000531.8−280553	1.20	0.46	0.07	16.08	15.15	17.21	12.74	*	15.28	53	9	Im	N	726	7.70	TF
AGC 748778	000634.4+153039	0.32	0.52	0.28	20.28	18.90		16.29	*	18.21	16	10	Ir	L	258	5.40	h′
And XX	000730.7+350756	0.80	0.70	0.25	21.84	19.00		14.67	*			−3	Sph	X		0.80	TRGB
UGC 00064	000744.0+405232	1.66	0.56	0.34	16.59	15.50		12.84	*	14.30	60	10	Ir	N	305	9.60	TF
ESO 349−031	000813.3−343442	1.23	0.82	0.05	17.14	15.71	21.43	13.02		15.53	30	10	Ir	L	221	3.21	TRGB
NGC 0024	000956.4−245748	7.24	0.22	0.08	14.16	12.38	16.03	8.96		13.54	213	5			550	9.90	TF
NGC 0045	001403.9−231056	8.51	0.69	0.09	12.69	11.55	14.41	9.09		11.98	172	8			465	9.20	TF

(This table is available in its entirety in machine-readable and Virtual Observatory (VO) forms in the online journal. A portion is shown here for guidance regarding its form and content.)

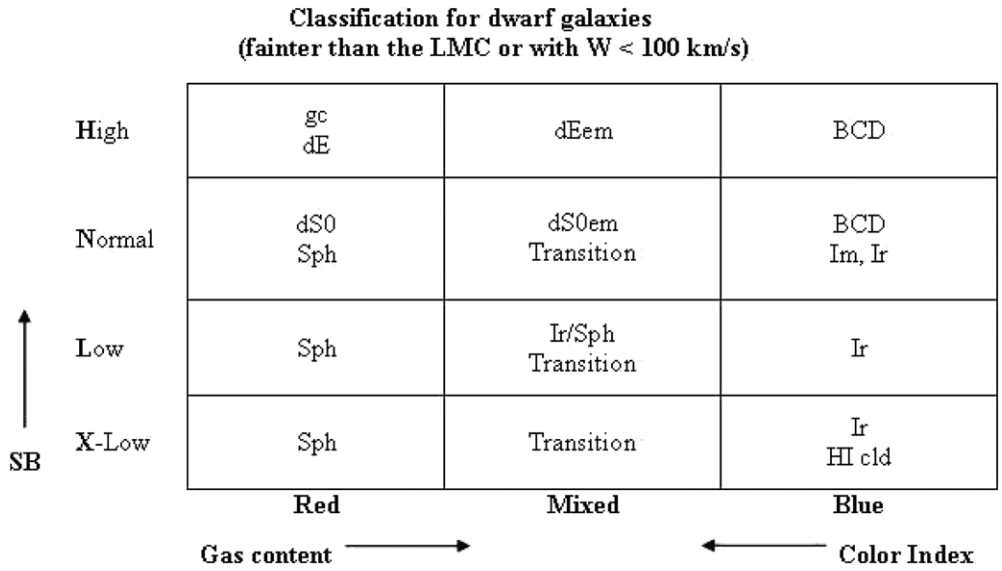

Figure 2. Classification of dwarf galaxies, which takes into account galaxy color or gas content as well as surface brightness. The upper left corner potentially includes globular clusters, and the opposite right bottom one may contain intergalactic H I clouds.

galaxies are given in Table 3 along with the measurement errors. For many galaxies their Hα line images are presented in our LV database.

9. Apparent magnitude of the galaxy in the near-infrared K_s band. The source of the K_s data is the 2MASS sky survey (Jarrett et al. 2000, 2003) supplemented by photometric measurements from Fingerhut et al. (2010) and Vaduvescu et al. (2005, 2006). Given the lack of accurate photometry, K magnitudes were estimated by apparent magnitudes in the optical (B, V, R, I) or near-infrared (J, H) bands using the synthetic color indices of galaxies from Buzzoni (2005) and Fukugita et al. (1995). If a galaxy had only a B magnitude, its K magnitude was determined by the relation between the average color index $\langle B-K\rangle$ and morphological type (Jarrett et al. 2003): $\langle B-K\rangle = 4.10$ for early types E, S0, Sa; $\langle B-K\rangle = 2.35$ for late types Sm, blue compact dwarf (BCD), Ir; and $\langle B-K\rangle = 4.60–0.25\cdot T$ for intermediate types $T = 3$–8 according to the de Vaucouleurs scale (marked by an asterisk).
10. Apparent magnitude of galaxy in the H I line

$$m_{21} = 17.4 - 2.5\log F_{\rm H\,I}, \qquad (4)$$

where the integral H I flux is expressed in Jy km s^{-1}. References to data sources on $F_{\rm H\,I}$ are listed in Table 3 and in the LV database.

11. H I line width in km s^{-1}, measured at the 50% level from the maximum. The main source of W_{50} data was LEDA, as well as the HIPASS and ALFALFA surveys. The references to individual W_{50} measurements are presented in Table 5 and the LV database.
12. Morphological type of galaxy in the numerical code according to the classification by de Vaucouleurs et al. (1991). It should be noted that about three quarters of objects in the LV are dwarf galaxies, which require a more detailed morphological classification. For example, dwarf spheroidal galaxies and normal ellipticals are usually denoted by the same numerical code $T < 0$, although their physical properties drastically differ. The classification problem arises as well for the "transient" type dwarf galaxies, Tr, which combine the features of spheroidal (Sph) and irregular (Ir) systems. Due to small classification errors, such objects may "jump" from one end of the T scale to the other.
13. and 14. In order to describe the morphology of dwarf galaxies in more detail, we introduce a two-parameter scheme, which takes into account both the surface brightness of a dwarf system: H—high; N—normal; L—low; X—extremely low, and its color (or the presence of emission): Ir, Im, BCD—blue; Tr, dS0em, dEem—mixed; and Sph, dE—red. This diagram is schematically shown in Figure 2 in the figure's lower right corner. The intergalactic H I clouds may be located and intergalactic globular clusters may be located in the upper left. Our classification within this scheme does not claim special evolutionary significance, but rather allows us to reflect the structure of galaxies with a luminosity below that of the LMC more accurately.
15. Heliocentric radial velocity in km s^{-1}. References to them are given in Table 4. As a rule, we selected the value of V_h having the smallest measurement error.
16. and 17. Distance to galaxy in Mpc, indicating the method used: (TRGB)—by the tip of the red giant branch; (Cep)—from the Cepheid luminosity; (geom)—by a geometric determination of the distance; (SN)—from the supernova luminosity; (SBF)—from galaxy surface brightness fluctuations; (mem)—from galaxy membership in known groups with measured distances of other members; (TF, FP)—by the Tully–Fisher relation or by the fundamental plane; (BS)—by luminosity of the brightest stars; (CMD)—by the color–magnitude diagram using some prominent features or simultaneous distance and stellar population fitting; (HB)—by the horizontal branch; (RR)—from the luminosity of RR Lyrae stars; (PNLF)—by the planetary nebula luminosity function; (h, h′)—by the Hubble velocity–distance relation at $H_0 =$ 73 km s^{-1} Mpc^{-1}, not accounting for (h) or in view of (h′) a certain Virgocentric flow model. In addition, we included in our sample a small number of dwarf galaxies ($N = 11$) that are missing the measurements of both optical and H I velocities due to their low surface brightness and H I deficiency. The texture of these objects indicates their likely proximity, which can be verified by future

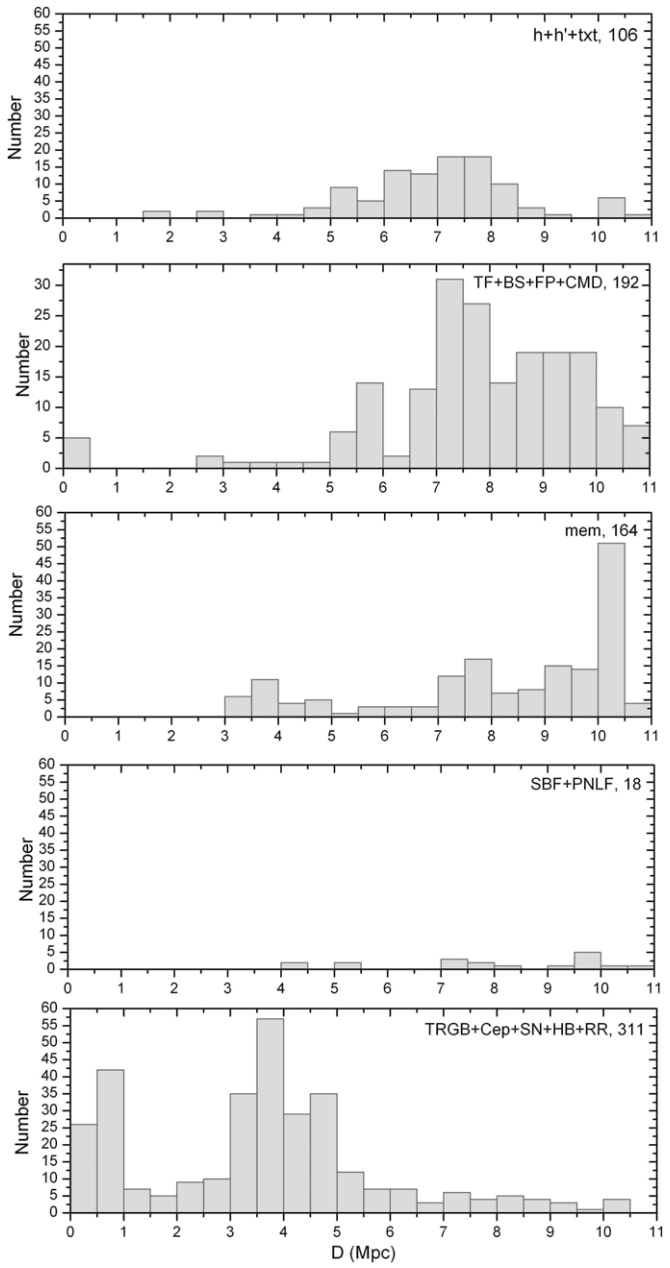

Figure 3. Distribution of 756 nearby galaxies according to their distance estimates derived by different methods.

observations with *HST*. These cases are designated in Column 17 as (txt). References to the distance estimation are presented in Table 6.

Figure 3 presents the distribution of galaxies based on their distance estimates, performed by various methods. For obvious reasons, the distance medians of these panels substantially vary for different methods. The smallest median of $D \sim 4$ Mpc falls within the subsample {rgb + cep + SN}, where the accuracy of distance measurements is the highest, amounting to 5%–10%.

We used the original observational data of nearby galaxies, compiled in Table 1, to calculate their linear diameter, integral luminosity, hydrogen mass, and other global parameters. These characteristics are presented in Table 2, where the columns contain:

1. Name of galaxy; in some cases (SDSS, APM, etc.) the coordinate part of name was reduced.
2. Equatorial coordinates for epoch J2000.0.
3. Major linear diameter (in kiloparsecs) at the Holmberg isophote, corrected for Galactic extinction and inclination according to Fouqué & Paturel (1985).
4. Inclination of galaxy i from the face-on position in degrees,

$$\sin^2 i = [1 - (b/a)^2] \cdot \left[1 - (b/a)_o^2\right]^{-1}, \quad (5)$$

where the intrinsic axial ratio of galaxy $(b/a)_o$ depends on its morphological type T as

$$\begin{aligned} \log(a/b)_o &= 0.43 + 0.53T \quad \text{for } T \leqslant 8 \\ \log(a/b)_o &= 0.38 \quad \text{for } T = 9, 10. \end{aligned} \quad (6)$$

We adopted this expression from Paturel et al. (1997) with a correction for the slight difference between our type scale and the LEDA T scale. Therefore, for the Ir, Im, and BCD-type galaxies we assume the intrinsic axial ratio to be $(b/a)_o = 0.42$ in accordance with the statistics of apparent axial ratios of these galaxies.
5. Amplitude of rotational velocity of galaxy $V_m = W_{50}^c/2 \sin i$, adjusted for the inclination, where the H I line width, W_{50}^c, contains a correction for turbulent motions following the Tully & Fouqué (1985) scheme with a parameter $\sigma_z = 10$ km s^{-1}.
6. Internal extinction in the galaxies in the B band according to Verheijen (2001):

$$A_B^i = [1.54 + 2.54(\log 2V_m - 2.5)] \log(a/b), \quad (7)$$

if $2V_m > 78$ km s^{-1}, otherwise $A_B^i = 0$. Therefore, dwarf galaxies with $V_m < 39$ km s^{-1}, gas-poor E, and S0 galaxies without W_{50} estimates, were considered to be fully transparent systems.
7. Absolute B-band magnitude of galaxies, corrected for Galactic and internal extinction.
8. Average surface brightness in the B band within the Holmberg isophote (mag arcsec^{-2})

$$\mathrm{SB}_B = B_T^c + 5 \log a_{26}^c + 8.63, \quad (8)$$

where the apparent magnitude and angular diameter are corrected for extinction and inclination.
9. Logarithm of K_s-band luminosity of the galaxy in solar units, corrected for extinction $K - K^c = 0.085(A_B^G + A_B^i)$, at absolute magnitude of the Sun $M_K^\odot = 3.28$ (Binney & Merrifield 1998).
10. Logarithm of the indicative mass M_{26} within the Holmberg radius, where the mass

$$M_{26} = 3.31 \cdot 10^4 V_m^2 \cdot a_{26}^c \cdot D \quad (9)$$

is expressed in solar masses, corrected angular diameter in arcminutes, V_m in km s^{-1}, and D in Mpc (Roberts & Haynes 1994).
11. Logarithm of hydrogen mass

$$M_{\mathrm{H\,I}} = 2.356 \cdot 10^5 \cdot D^2 \cdot F_{\mathrm{H\,I}}, \quad (10)$$

where $M_{\mathrm{H\,I}}$ is expressed in solar masses, D in Mpc, and $F_{\mathrm{H\,I}}$ in Jy km s^{-1} (Roberts & Haynes 1994).

Table 2
Global Parameters of the Nearby Galaxies

Name	R.A. J2000.0 Decl.	A_{26}	i	V_m	A_B^i	M_B^c	SB_B	$\log L_K$	$\log M_{26}$	$\log M_{H\,I}$	V_{LG}	Θ_1	MD	Θ_5	Θ_j
(1)	(2)	(3)	(4)	(5)	(6)	(7)	(8)	(9)	(10)	(11)	(12)	(13)	(14)	(15)	(16)
UGC 12894	000022.5+392944	2.78	33	21	0.00	−13.3	25.2	7.58	8.17	7.92	619	−1.5	NGC 7640	−1.2	
WLM	000158.1−152740	3.21	90	22	0.00	−14.1	24.8	7.69	8.27	7.83	−16	0.0	MESSIER031	0.2	1.74
And XVIII	000214.5+450520	0.63	10		0.00	−9.1	26.2	6.60			−44	0.4	MESSIER031	0.5	1.52
ESO 409−015	000531.8−280553	2.65	78	23	0.00	−14.4	24.1	7.99	8.20	7.99	769	−1.7	NGC 0253	−1.2	
AGC 748778	000634.4+153039	0.53	70	3	0.00	−10.0	24.9	6.27	5.64	6.51	486	−1.6	NGC 0253	−1.3	
And XX	000730.7+350756	0.20	58		0.00	−5.8	27.0	5.26			−182	2.4	MESSIER031	2.4	1.74
UGC 00064	000744.0+405232	4.87	66	28	0.00	−14.8	25.0	8.15	8.65	8.58	587	−1.7	DDO 217	−1.3	−1.15
ESO 349−031	000813.3−343442	1.15	39	14	0.00	−11.9	24.7	7.12	7.41	7.13	230	0.0	NGC 0253	0.1	0.51
NGC 0024	000956.4−245748	19.98	85	95	0.64	−18.3	24.5	9.75	10.32	8.91	606	−1.0	NGC 0045	−0.8	0.42
NGC 0045	001403.9−231056	22.88	47	103	0.17	−18.5	24.6	9.61	10.45	9.47	528	−0.9	NGC 0024	−0.8	0.51

(This table is available in its entirety in machine-readable and Virtual Observatory (VO) forms in the online journal. A portion is shown here for guidance regarding its form and content.)

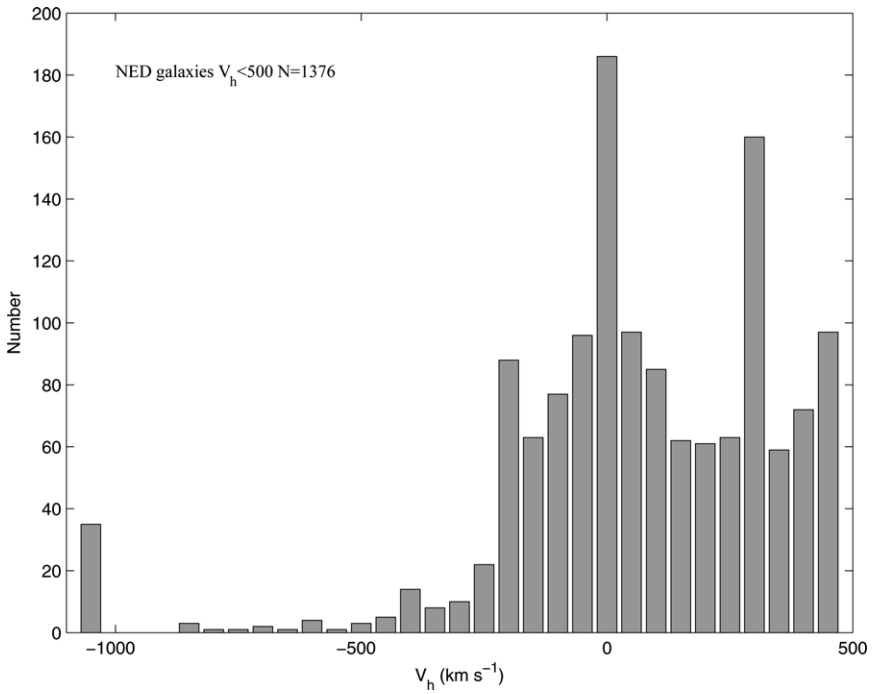

Figure 4. Number vs. heliocentric velocity distribution for 1376 non-galaxy objects with low velocities from automatic surveys indicated in NED as "galaxies."

12. Radial velocity of the galaxy relative to the Local Group centroid with apex parameters (Karachentsev & Makarov 1996) adopted from NED:

$$V_{\rm LG} = V_h + 316[\sin b \cdot \sin(-4^\circ) + \cos b \cdot \cos(-4^\circ) \cdot \cos(l - 93^\circ)], \quad (11)$$

where l and b are Galactic coordinates of the galaxy.
13. Tidal index Θ_1, determined below in Section 8 via distance and mass of the nearest significant neighbor. Positive values of Θ_1 indicate the membership in groups; negative values correspond to isolated galaxies.
14. Name of the "main disturber"(MD), i.e., the neighboring galaxy, producing the maximal tidal influence on the galaxy. In fact, the set of objects in Table 2 with the same MD and $\Theta_1 > 0$ corresponds to a definition of the physical group of the galaxies.
15. Another tidal index (or density contrast), determined by the five most important neighbors. Unlike Θ_1, the index Θ_5 seems to be a more robust feature of the galaxy environment.
16. Logarithm of the K-band luminosity density within 1 Mpc around the galaxy, taken in units of the mean global L_K density derived from the Two Micron All Sky Survey (2MASS) by Jones et al. (2006).

4. ON THE SAMPLE COMPLETENESS

The degree of completeness in the number of galaxies presented in a sphere of 10 Mpc radius can only be estimated approximately, since it depends on many factors which are hard to verify. The optical and H I surveys of the sky are usually limited to a fixed flux, but the difference of the galaxies in luminosity, size, surface brightness, and gas abundance is enormous. High-accuracy distances to most of the galaxies are known as yet within ∼5 Mpc. Given the distance measurement errors by the Tully–Fisher method of ∼(20–25)%, a significant part of the galaxies at the periphery of the LV are only its conditional members. The presence of collective non-Hubble motions on the scale of ∼10 Mpc also makes it difficult to assess the completeness of our sample, since the amplitude of these motions (∼300 km s^{-1}) may make up half of the velocity constraint (1) that we have adopted. Note that the "Zone of Avoidance" behind the Milky Way is already well filled with nearby galaxies owing to the systematic surveys in the H I line.

We should note that evaluating the completeness of the LV sample is also affected by a problem of "astro-spam." Massive automatic surveys of galaxy redshifts produce a significant number of cases where the radial velocity of a star, projected onto a distant galaxy, is falsely attributed to this galaxy. For example, the DEEP2 spectral survey (http://deep.berkeley.edu) and other recent surveys give more than 1000 fictitious objects (see Figure 4) included in NED as "galaxies" with velocities $V_h < 500$ km s^{-1}. This implies that the amount of "rubbish" from the automatic surveys is greater than the actual population of the LV. Another source of astro-spam is the confusion in the optical identification of H I sources in surveys with low angular resolution. The presence around our Galaxy of hundreds of high-velocity clouds with low line-of-sight velocities and small W_{50} widths also provokes the inclusion of false "nearby" dwarf galaxies in the LV (plenty of such examples can be found in the paper by Côté et al. 1997). Finally, galaxy databases account for very exotic cases, for instance, the "galaxy" AM 0912-241 (see NED) with a radial velocity of +614 km s^{-1} (Mathews et al. 1995), which is in fact only a photographic emulsion defect.

Some idea of the completeness rate of the LV sample is given in Figure 5, where the panels demonstrate the distributions of galaxies by absolute B magnitude, linear diameter A_{26}, and line width W_{50} depending on distance. These data imply that the galaxies with absolute magnitudes brighter than $-11^{\rm m}$ or linear diameters $A_{26} > 1.0$ kpc occur as frequently in both the nearby and the distant parts of our sample. In this sense, the conditional level of completeness of the LV sample is about (40–60)%, which is indirectly confirmed by the distribution

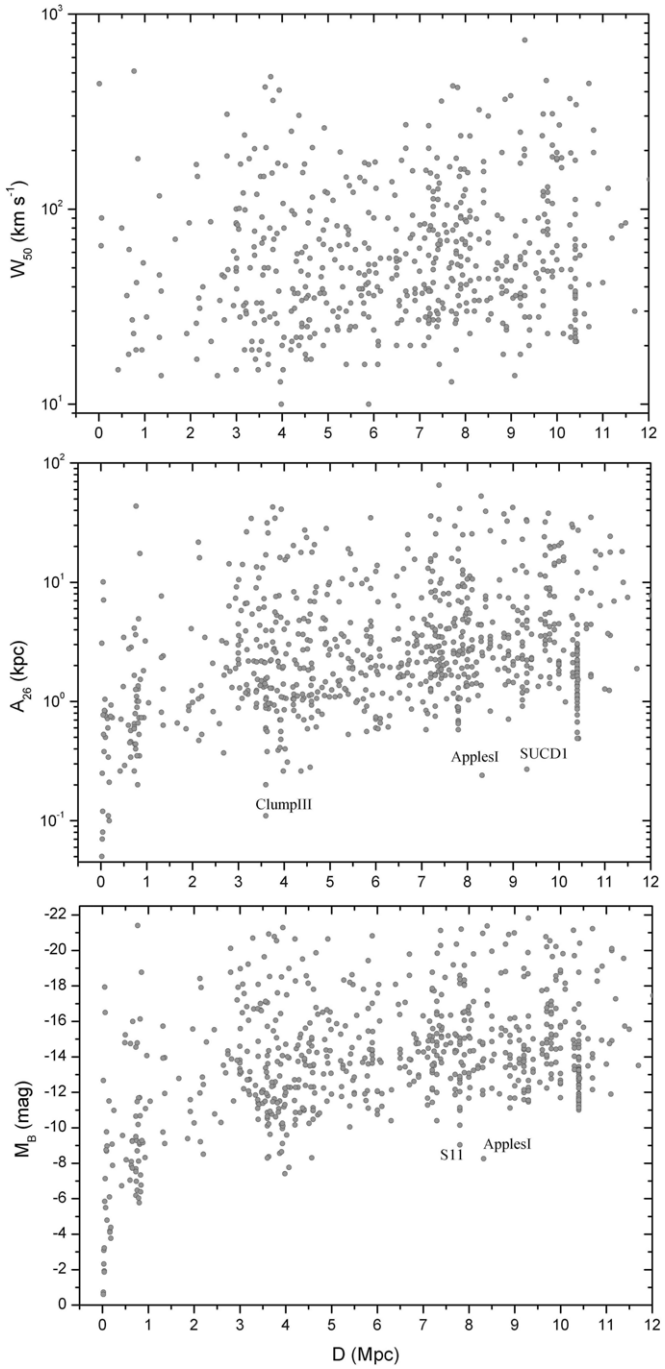

Figure 5. Distribution of nearby galaxies according to their absolute magnitude (bottom), linear Holmberg diameter (middle), and H I line width (top). Some ultra-faint dwarfs are denoted.

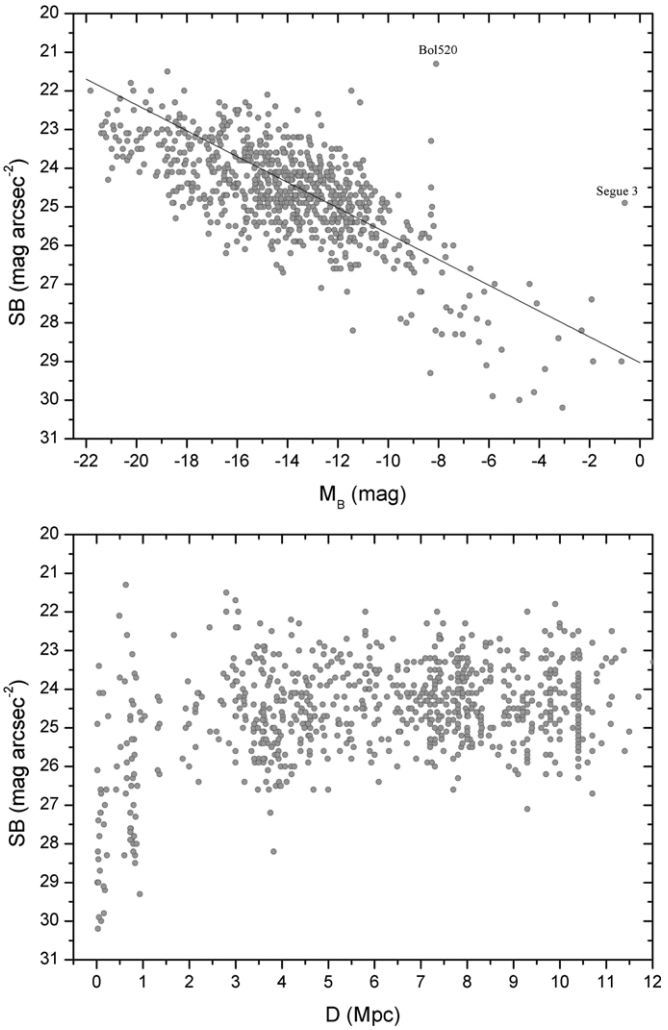

Figure 6. Mean surface brightness of the LV galaxies vs. their absolute magnitude (bottom) and distance (top). The line traces a case of constant spatial luminosity density within the Holmberg radius.

of W_{50} versus D. However, among the members of the Local Group ($D < 1$ Mpc), only half of the galaxies have absolute magnitudes brighter than $-11^{\rm m}$. Consequently, more than half of the ultra-faint dwarf companions around normal galaxies, like the Sombrero galaxy ($D = 9.3$ Mpc), still remain outside our field of view.

The case of the isolated dwarf spheroidal galaxy Apples I with $M_B^c = -8^{\rm m}.30$ and $A_{26}^c = 0.25$ kpc at a distance of 8.5 Mpc is intriguing here. This galaxy was accidentally discovered by Pasquali et al. (2005) as a system resolved into stars with *HST*. The statistics of images obtained so far with *HST* shows (Karachentsev et al. 2009) that the population of such difficult-to-detect tiny crumbs without gas and with only an old stellar population may reach up to $N \sim 10^3$–10^4 in the LV, i.e., be dominant over other types of galaxies.

The upper panel in Figure 6 shows the distribution of mean surface brightness of the LV galaxies at different distances. If we exclude the dwarf systems of the Local Group with SB > 26.5 mag arcsec^{-2}, then the mean surface brightness is almost independent of distance. Dwarf companions of the Andromeda and Milky Way with SB $= (27$–$31)$ mag arcsec^{-2} are distinguishable at close distances only due to the fact that they are resolved into individual stars. It is obvious that a large number of such satellites can also exist around more distant normal galaxies. A special survey of similar objects in a region of the M 81 group (Chiboucas et al. 2009) confirms this assumption.

In cosmological models, describing the structure of dark galaxy halos, the central density of matter is presumed to be the same regardless of the size and mass of the halo (Navarro et al. 1996). As such, the mass and size of the halos are related as $M_{\rm DM} \sim R^3$. If the distribution of stellar matter follows the distribution of dark matter, we can expect a similar relation $L \sim A^3$ between the integral luminosity of galaxy and its diameter, which implies the relation SB $\sim (1/3)\, M_B$. Such a relationship is indicated at the bottom plot of Figure 6 by the

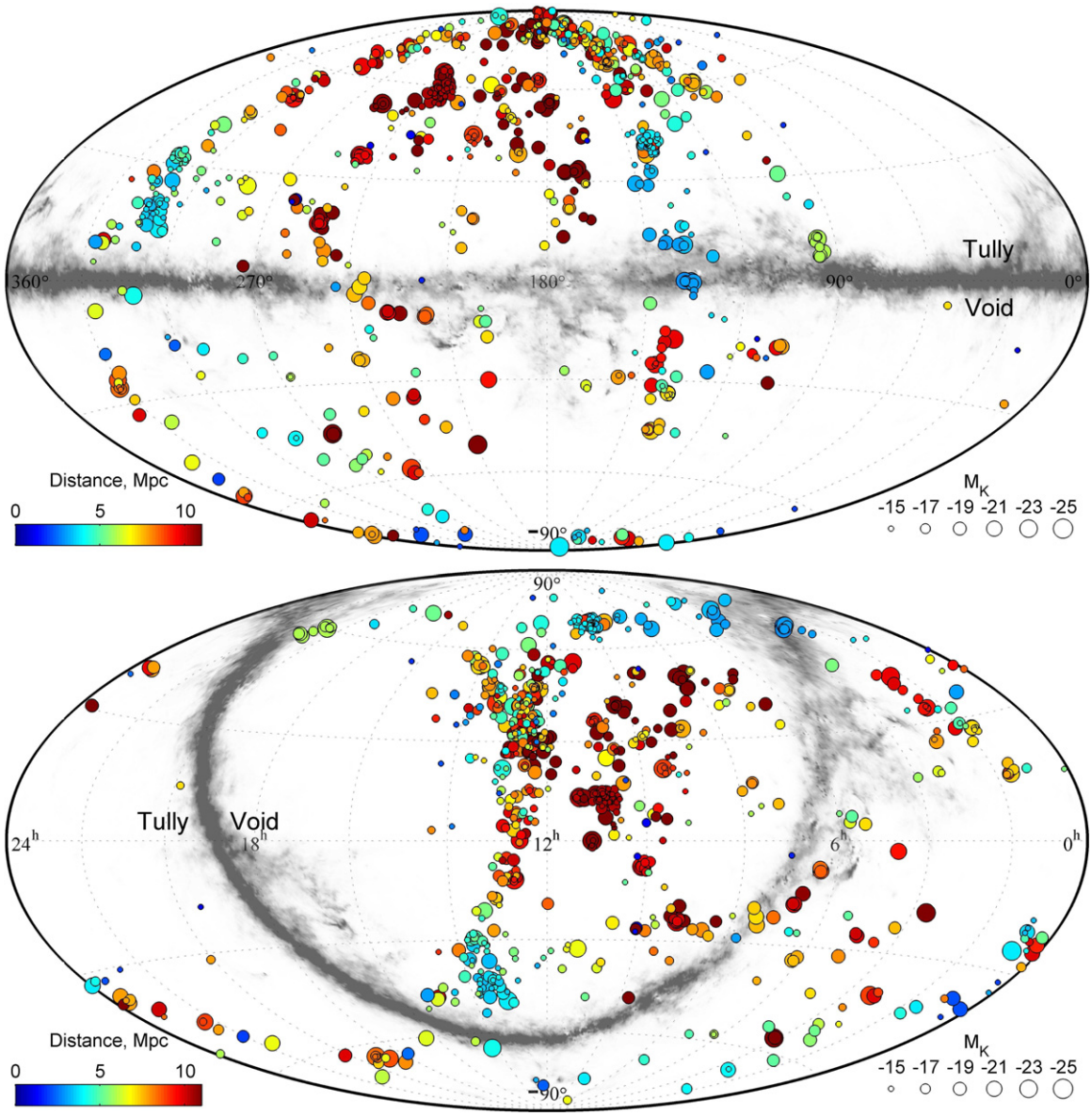

Figure 7. Distribution of nearby galaxies on the sky in equatorial (bottom) and galactic (top) coordinates. The Local Group members are not shown. Galaxy distance and luminosity are indicated by circles of different colors and sizes. The zone of avoidance in the Milky Way is outlined by the gray stripe.

(A color version of this figure is available in the online journal.)

straight line. As one can see, the LV sample as a whole follows the expected relation fairly well. The deviation from it at the extremely low surface brightness end is due to a systematic overestimation of dwarf galaxy sizes, the brightness profiles of which lie entirely below the Holmberg isophote.

5. GALAXY DISTRIBUTION WITHIN 11 Mpc

The distribution of the LV galaxies on the sky is shown in Figure 7 in equatorial (bottom panel) and galactic (top panel) coordinates. The galaxies with distances of $D = (1–11)$ Mpc are shown by circles, whose size reflects the luminosity of galaxy and whose color reflects distance. Here the members of the Local Group with $D < 1$ Mpc were excluded. The smeared gray stripe in the panels corresponds to the region of strong extinction in our Galaxy. The distribution of galaxies shows their concentration in the region of well-known nearby groups around M 81, Centaurus A, M 83, IC 342, NGC 253, M 101, NGC 6946, Leo I, etc. The figure exhibits an extensive area in the Hercules-Aquila, almost completely devoid of galaxies, i.e., the Local Void (Tully 1988). This void extends far beyond the LV boundary.

The distribution of galaxies within a sphere of 11 Mpc radius is shown in the panels of Figure 8 in different projections of Cartesian Supergalactic coordinates SGX, SGY, and SGZ. The size of the circles characterizes the luminosity of the galaxies and their color marks the peculiar velocity $V_{\rm pec} = (V_{\rm LG} - 73 \cdot D)$ according to the scale between the panels. The clustering of galaxies in groups as well as toward the supergalactic plane is clearly noticeable. These panels show that the galaxies with high negative peculiar velocities are located far away from the supergalactic plane, and the galaxies with $V_{\rm pec} > +300$ km s^{-1} are concentrated in the region of SGY > 6 Mpc, showing the tendency of infall toward the Virgo cluster (its coordinates are SGY $= +16$ Mpc, SGX $\simeq$ SZY $\simeq 0$). These data give us the

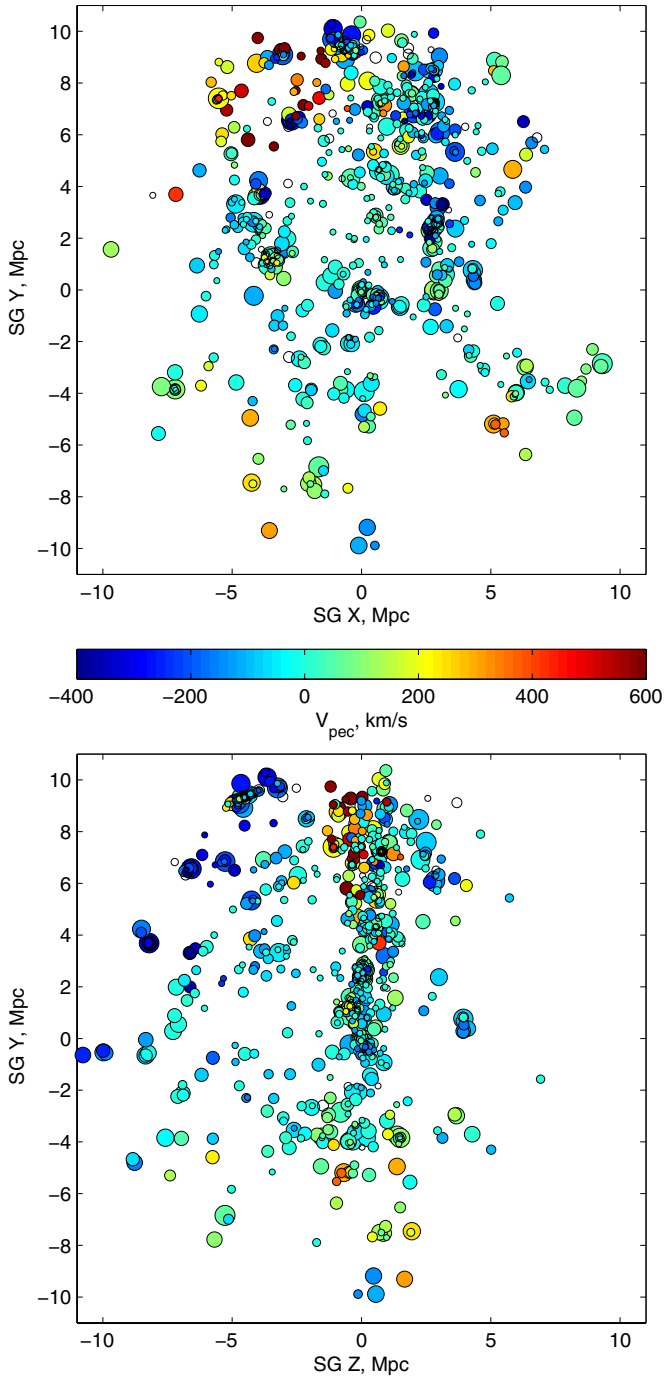

Figure 8. Distribution of the LV galaxies within 11 Mpc in Cartesian supergalactic coordinates. The luminosity of the galaxies is marked by the size of circles, and peculiar velocities are indicated by the color scale.

(A color version of this figure is available in the online journal.)

idea that the pattern of motions in the LV is rather far from the unperturbed Hubble flow.

6. MORPHOLOGY AND OPTICAL SCALING RELATIONS

It is well known that both the galaxies with a dominant disk ($T > 3$) and those with a dominant bulge ($T < 4$) tend to be located along some "fundamental plane" in the parameter space (luminosity–dimension–internal motion amplitude). Three projections of this distribution in the coordinates (M_B, A_{26}, V_m) are shown in the panels of Figure 9. Late-type galaxies ($T > 3$) are marked by solid circles, while the objects of early types are denoted with open ones. The most distinct correlation is visible between the linear diameter and the absolute magnitude of the galaxies (the bottom panel). The straight line there corresponds to the constant spatial luminosity density within the Holmberg isophote, $\log A_{26} \propto -(2/15)\, M_B$, which is followed

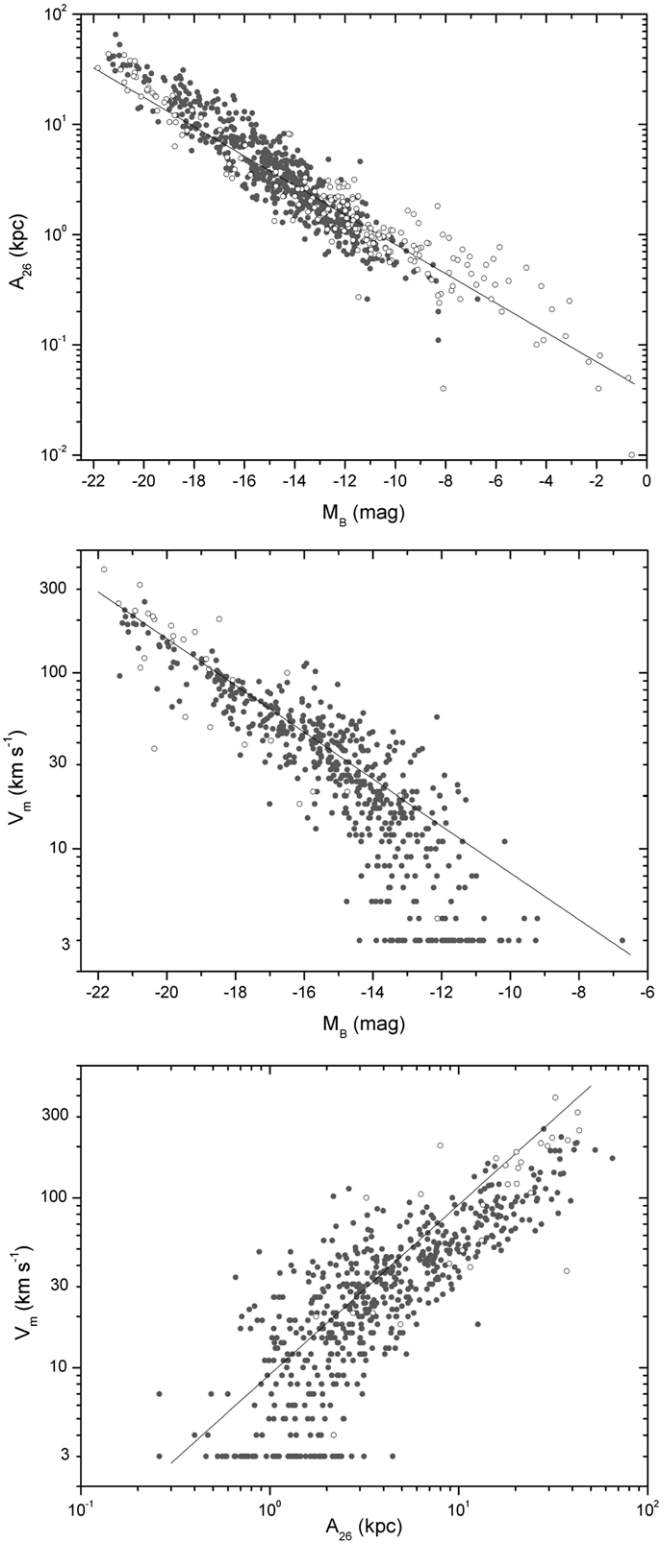

Figure 9. Scaling relation between the absolute magnitude, Holmberg diameter, and rotation velocity for the LV galaxies. Late-type ($T > 3$) galaxies are shown by filled circles and early-type galaxies are represented by open ones.

by the galaxies only in the first approximation. Recall that the diameters of the faint dwarf spheroidal satellites of the Milky Way and Andromeda were estimated at this level, which is much fainter than the Holmberg isophote.

The relation between the rotation amplitude of galaxy and its absolute magnitude is shown in the middle panel. The straight line represents a cubic relation, $L_B \sim V_m^3$, which is also known as the blue Tully–Fisher relation, $M_B \sim -7.5 \log V_m$. The dwarf galaxies in the lower right corner of the diagram systematically deviate from the regression line for normal spirals. In dwarf galaxies having a rotation velocity less than 30 km s^{-1} the turbulent gas motions with a typical value of about 10 km s^{-1} play a significant role in the mass determination. Careful account for that effect could straighten the Tully–Fisher relation in a broader range of luminosity.

The upper panel of Figure 9 shows that the correlation between the galaxy's dimension and the amplitude of its rotation follows the expected linear relation $V_m \propto A_{26}$ (direct line) only in a rough approximation. The dispersion in this diagram is greater than in the previous two. Perhaps one can find other observational parameters, say, a half-luminosity radius and a quadratic sum of rotational and turbulent velocities, which yield this relation to be more linear and less scattered.

Luminosity, dimension, and rotation amplitude are different for galaxies of different morphological types. Their distributions along the T scale are shown in three panels of Figure 10. For each global parameter: M_B, A_{26}, and V_m, the average value as a function of T has an approximately parabolic shape with the maximum located at type $T \simeq 4$, i.e., Sbc. The scatter of all three parameters near the maximum is minimal, which is probably caused by specific dynamic conditions intrinsic to this type of galaxy. Note that in the V_m versus T diagram, the number of galaxies left of the peak is much smaller than in the two bottom panels, i.e., A_{26} and M_B. A low content of gas in early-type galaxies does not usually allow us to measure rotation amplitude accurately in them, which can introduce a significant hidden selection in the analysis of diagrams similar to Figure 9.

It should be noted that in the Hubble morphological classification scheme, the type of dwarf irregular galaxy was a sort of "trash bin" where the "ugly" objects were dropped. However, three-fourths of the sample of the LV consists of dwarf galaxies. One can see from the previous figure that the distribution of M_B, A_{26}, and V_m parameters merges into a thick lane, denoting the need of a more refined classification of dwarf systems. The two-dimensional classification (Figure 2) that we propose is based on the difference in their color (or the presence of emission) and surface brightness. Figure 11 shows the distribution of a number of dwarf objects in our scheme by type. The cells of the scheme vary considerably in the degree of filling, which is obviously caused by conditions of dwarf system formation and subsequent evolution in different environments. However, the two-dimensional shape of this diagram may be subject to a significant selection effect: the galaxies poor in gas and of extremely low surface brightness, such as Apples I, can easily stay undetected both in the optical and H I surveys. It follows from the histograms of Figure 12 that though the distributions of dwarf galaxies overlap by visual surface brightness gradations, they have a distinct median trend on the SB scale (mag arcsec^{-2}): 23.0 (H), 24.2 (N), 25.2 (L), and 27.6 (X). Observed differences in the mean surface brightness of dwarf galaxies reach more than 10 mag, and these differences are obviously caused by features of star formation history in them.

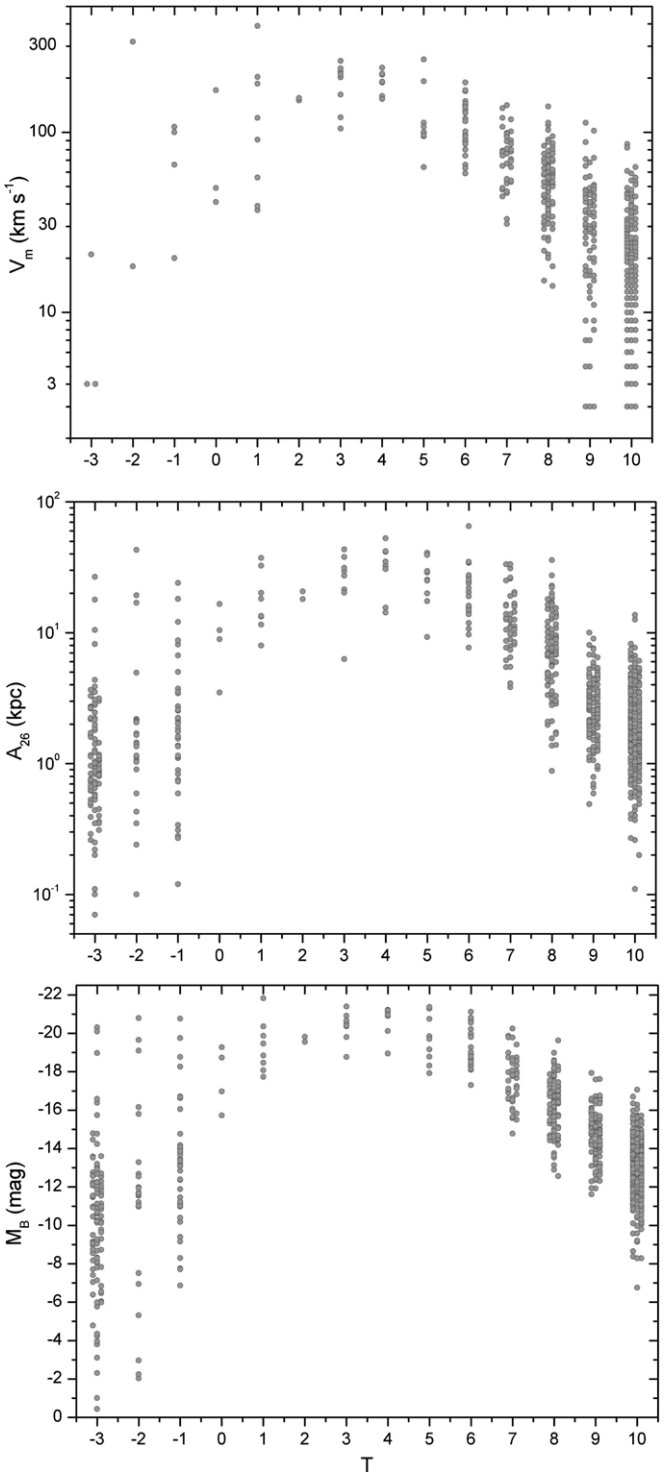

Figure 10. Absolute magnitude, Holmberg diameter, and rotation velocity of the LV galaxies as a function of their morphological type.

An important dynamic characteristic of galaxies is the ratio of their indicative mass within the Holmberg isophote to the total luminosity. Figure 13 represents the distribution of this ratio in the B and K bands for different morphological types. The galaxies with inclination angles $i < 45^\circ$, for which the estimate of M_{26} may contain a considerable uncertainty, are marked with empty symbols. Both ratios show a growth trend from early to late types, more pronounced in the case of the ratio M_{26}/L_K. However, in the transition from spiral galaxies

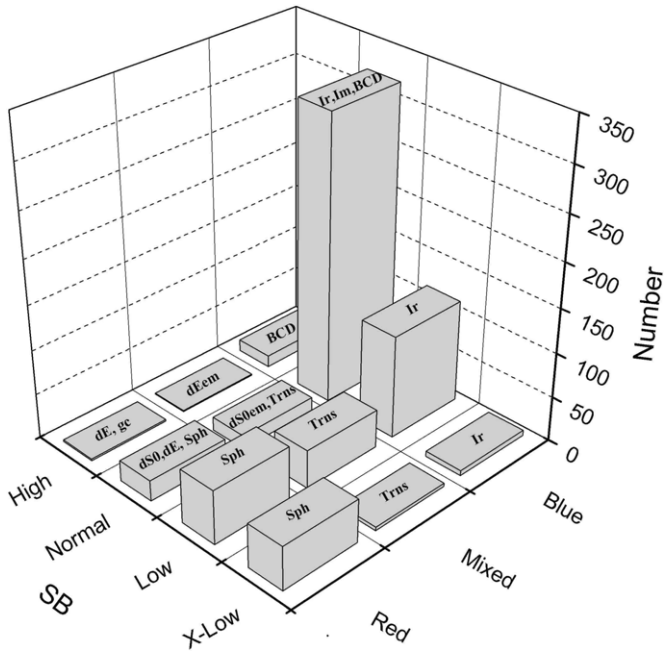

Figure 11. Same classification of dwarf galaxies as in Figure 2, but with indication of the LV galaxy number in each morphological cell.

(Sd, Sm) to irregulars (BCD, Im, Ir), there is a significant (about four-fold) decrease in the average M_{26}/L ratio. This effect may be due to a difference in structure and kinematics of galaxies in the presence or absence of spiral pattern, in particular owing to the contribution of turbulent motions, which is ignored in the evaluation of mass M_{26} by Equation (9).

7. MAIN H I PROPERTIES OF THE LV SAMPLE

Hydrogen characteristics of different samples of galaxies, limited by H I flux, apparent magnitude, or angular diameter of galaxies, have been repeatedly investigated (Roberts & Haynes 1994; Zwaan et al. 2003; Martin et al. 2010). These samples have a strong bias toward the disk-shaped galaxies of high luminosity and do not reflect the H I properties of galaxies in the unit volume, dominated by dwarf objects. Currently, more than 70% of the LV galaxies are detected in the H I line, and an upper limit of H I fluxes is known for another ∼14% of these galaxies. Huge progress has been made here via the massive H I surveys on the Parkes (HIPASS) and Arecibo (ALFALFA) radio telescopes, and within a special survey of nearby dwarf galaxies, performed by Huchtmeier in Effelsberg. However, at high declinations (decl. $> +38^\circ$) there are still a number of nearby galaxies not observed in the H I line. The planned "blind" H I survey of the northern sky (WNSHS) at Westerbork (http://www.astron.nl/jozsa/wnshs/) will obviously fill this gap shortly.

Figure 14 represents the ratio of hydrogen mass to B- and K-band luminosity versus the rotation amplitude of galaxies V_m (lower and middle panels). The sample of nearby galaxies demonstrates the well-known effect that the average ratio $M_{\rm H\,I}/L_B$ increases from $\sim 0.1\,M_\odot/L_\odot$ to $\sim 0.7\,M_\odot/L_\odot$ in the transition from normal spiral galaxies to dwarf systems with $V_m < 50$ km s^{-1}. This feature is usually attributed to the lower rate of star formation in dwarf galaxies with their turbulent motions compared to the disks, where regular rotation and density waves boost the process of star formation. Note that the smallest dwarfs with $V_m < 6$ km s^{-1} show some tendency of decreasing the $M_{\rm H\,I}/L$ ratio. Perhaps this is due to the fact that a shallow potential well in dwarf systems is not capable of retaining large masses of gas.

The K-band luminosity of galaxies is a good indicator of their stellar mass, M_*, since it is almost insensitive to internal extinction and the presence of young stellar population. At $M_*/L_K \simeq 1\,M_\odot/L_\odot$ (Bell et al. 2003) the $M_{\rm H\,I}/L_K$ ratio in the middle panel of Figure 14 is actually equivalent to the mass ratio of gas and stars in the galaxies. For dwarf galaxies with $V_m < 50$ km s^{-1}, the average $M_{\rm H\,I}/L_K$ ratio amounts to $\sim 0.7\,M_\odot/L_\odot$. Taking into account a correction for abundances of helium and molecular gas, $M_{\rm gas} = 1.85 M_{\rm H\,I}$ (Fukugita & Peebles 2004), we obtain the characteristic ratio of $M_{\rm gas}/M_* = 1.3$ for dwarf galaxies. Hence, more than a half of the baryon mass in dwarf galaxies, detected in H I, remains unprocessed into the stellar component.

The upper panel of Figure 14 shows the behavior of the hydrogen mass-to-dynamical mass ratio within a Holmberg radius depending on V_m. For normal spiral galaxies ($V_m > 100$ km s^{-1}) we have the median value of $M_{\rm H\,I}/M_{26} \sim 0.03$, while for the dwarf galaxies with $V_m < 20$ km s^{-1} it increases to $M_{\rm H\,I}/M_{26} \sim 1$, in some cases reaching $M_{\rm H\,I}/M_{26} > 10$. Only a small fraction of these extreme ratios is due to errors in determining the inclination angle i of the galaxy (the cases with $i < 45^\circ$ are marked in this panel with empty triangles).

As noted by Roberts & Haynes (1994), an important global parameter characterizing the conditions of star formation in a galaxy is its average surface density of hydrogen, $M_{\rm H\,I}/A_{26}^2$. The distribution of this parameter for the LV galaxies is represented in the panels of Figure 15 depending on the rotation amplitude V_m and morphological type T. In the $T \geqslant 0$ region, the mean density $M_{\rm H\,I}/A_{26}^2$ weakly increases toward the late types, showing the minimum variance around $T = 4$ (Sbc). Large variations in the surface density of hydrogen mass at both edges of the morphological scale are easily explained by some features of their evolution: the depletion of gas reserves in E and S0 galaxies, and the sweep-out of gas from dwarf systems during bursts of star formation and/or under their passage through the halo of massive galaxies. For the faintest dwarf galaxies with rotation velocities of $V_m < 6$ km s^{-1}, some noticeable decline of the average surface density of hydrogen mass is observed.

8. ENVIRONMENT AND GAS-TO-STAR TRANSFORMATION

Different indicators can be used for quantitative description of a galaxy environment density. Karachentsev & Makarov (1999), considering a galaxy "i," performed a ranking of its neighbors "n" by a tidal force magnitude $F_n \sim M_n/D_{\rm in}^3$, where $D_{\rm in}$ is the spatial distance of a neighboring galaxy and M_n is its mass, which is considered proportional to the galaxy luminosity. The local mass density was characterized by the "tidal" index

$$\Theta = \max\left[\log\left(M_n/D_{\rm in}^3\right)\right] + C, \quad n = 1, 2, \ldots, N \qquad (12)$$

of the most significant neighbor, called the "main disturber" (=MD). The value of constant $C = -10.96$ was chosen so that at $\Theta = 0$ the galaxy "i" is located on the "zero velocity sphere" relative to the MD. At that, the galaxies with $\Theta > 0$ turned out to be members of a certain group, and the negative values of Θ corresponded to isolated galaxies.

For each galaxy of the LV, we calculated the tidal index Θ_1 according to Equation (12), considering the masses of galaxies to be proportional to their K luminosities. The value of the Θ_1

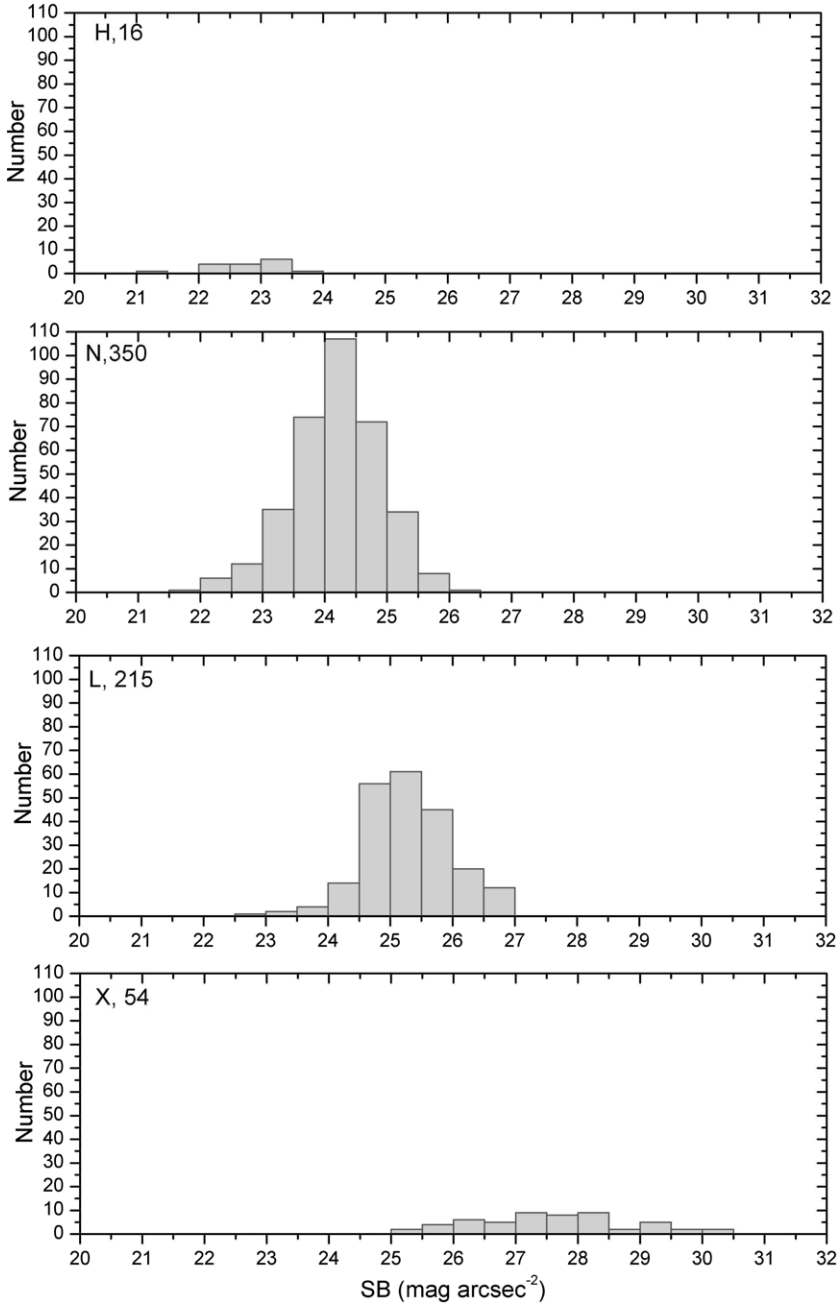

Figure 12. Distribution of 605 dwarf galaxies in the LV according to their mean surface brightness. Galaxies classified as having extremely low (X), low (L), normal (N), and high (H) surface brightness are presented in different panels.

index and the name of the MD are presented in Columns 13 and 14 of Table 2. The tidal index Θ_1 or actually a stellar density contrast, contributed by one, most important neighbor, i.e., MD, can significantly change with time due to orbital motions of galaxies. It therefore seems reasonable to use other parameters for characterizing the local environment. As a case of another more robust estimator, we calculated the index

$$\Theta_5 = \log\left(\sum_{n=1}^{5} M_n/D_{\rm in}^3\right) + C, \qquad (13)$$

which is the sum of the density contrasts produced by five most important neighbors. The value of constant C here is the same as in Equation (12).

Finally, in the last column of Table 2 we present the third environment estimator—the logarithm of the average density of the K luminosity of galaxies within the 1 Mpc radius sphere around the galaxy under consideration, expressed in units of the global mean density of K luminosity, $4.28 \times 10^8\ L_\odot\ {\rm Mpc}^{-3}$, derived from 2MASS (Jones et al. 2006):

$$\Theta_j = \log(j_K(1\,{\rm Mpc})/j_{K,{\rm global}}). \qquad (14)$$

Here, the central galaxy is not included in the estimate of average density. Note that in some galaxies no neighbors were detected within 1 Mpc and the Θ_j index for them is formally assumed to be -3.0.

Distributions of galaxies in the LV by the hydrogen mass-to-K-luminosity ratio and tidal index Θ_1, Θ_5, or Θ_j are presented

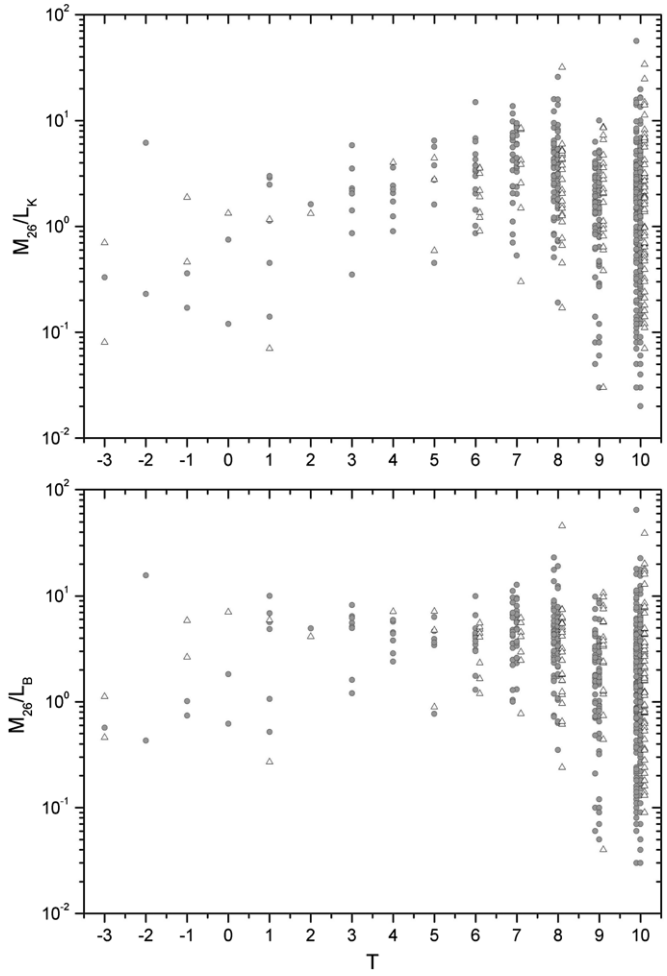

Figure 13. Indicative mass-to-luminosity ratio in B and K bands as a function of morphological type of the LV galaxies. Face-on galaxies with inclination $i < 45^\circ$ are shown by open triangles.

in Figure 16. Galaxies with the H I flux upper limit are shown by open circles. These data show that the maximum value of $M_{\rm H\,I}/L_K$ remains approximately the same for both the field galaxies and group members, regardless of the adopted density estimator: Θ_1, Θ_5 or Θ_j. In contrast, there is a steep drop in the minimum value of $M_{\rm H\,I}/L_K$ in the direction of high-density environments. It is obvious that the observed increase in H I deficiency toward a high-density environment is due to the sweep-out of gas from galaxies under their tight interaction. This process can reduce the amount of hydrogen in a galaxy by an order of two to four, thereby affecting the rate of star formation in it.

To estimate the integral star formation rate (SFR) in a galaxy, we used the relation

$$\mathrm{SFR}[M_\odot\ \mathrm{yr}^{-1}] = 0.945 \times 10^9 F_c(\mathrm{H}\alpha) D^2 \qquad (15)$$

from Kennicutt (1998), where D is the distance in Mpc and $F_c(\mathrm{H}\alpha)$ is the integral flux in the Hα line (erg cm^2 s^{-1}), corrected for Galactic and internal extinction as

$$A(\mathrm{H}\alpha) = 0.538\left(A_B^G + A_B^i\right). \qquad (16)$$

Values of the $F(\mathrm{H}\alpha)$ flux and apparent $m(\mathrm{H}\alpha)$ magnitudes in Table 1 are related by Equation (3).

The distribution of the specific SFR per unit of K luminosity of a galaxy is presented in three panels of Figure 17, depending

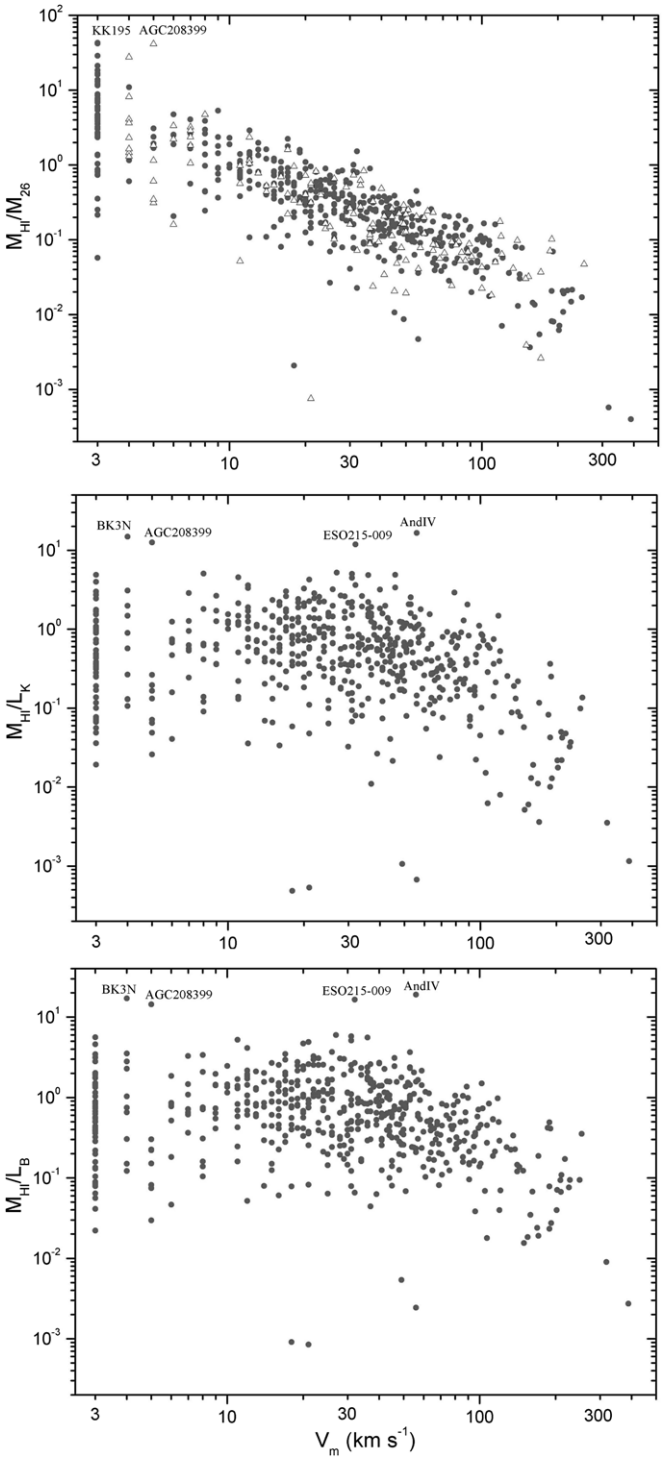

Figure 14. Hydrogen mass-to-luminosity ratio in B (bottom) and K bands (middle) vs. rotation velocity of the LV galaxies. The upper panel presents hydrogen mass-to-indicative mass for them. Face-on galaxies are marked by open triangles.

on Θ_1, Θ_5, and Θ_j as the argument. The shape of these diagrams is largely similar to the corresponding $M_{\rm H\,I}/L_K$ distributions in Figure 16. The increasing scatter of both $M_{\rm H\,I}/L_K$ and SFR$/L_K$ from isolated galaxies to group members provides evidence of a well-known fact that the environment of galaxies significantly affects the process of converting gas into stars.

To date, Hα fluxes are measured for 495 galaxies in the LV. The SFR estimates via Hα correspond to a timescale of

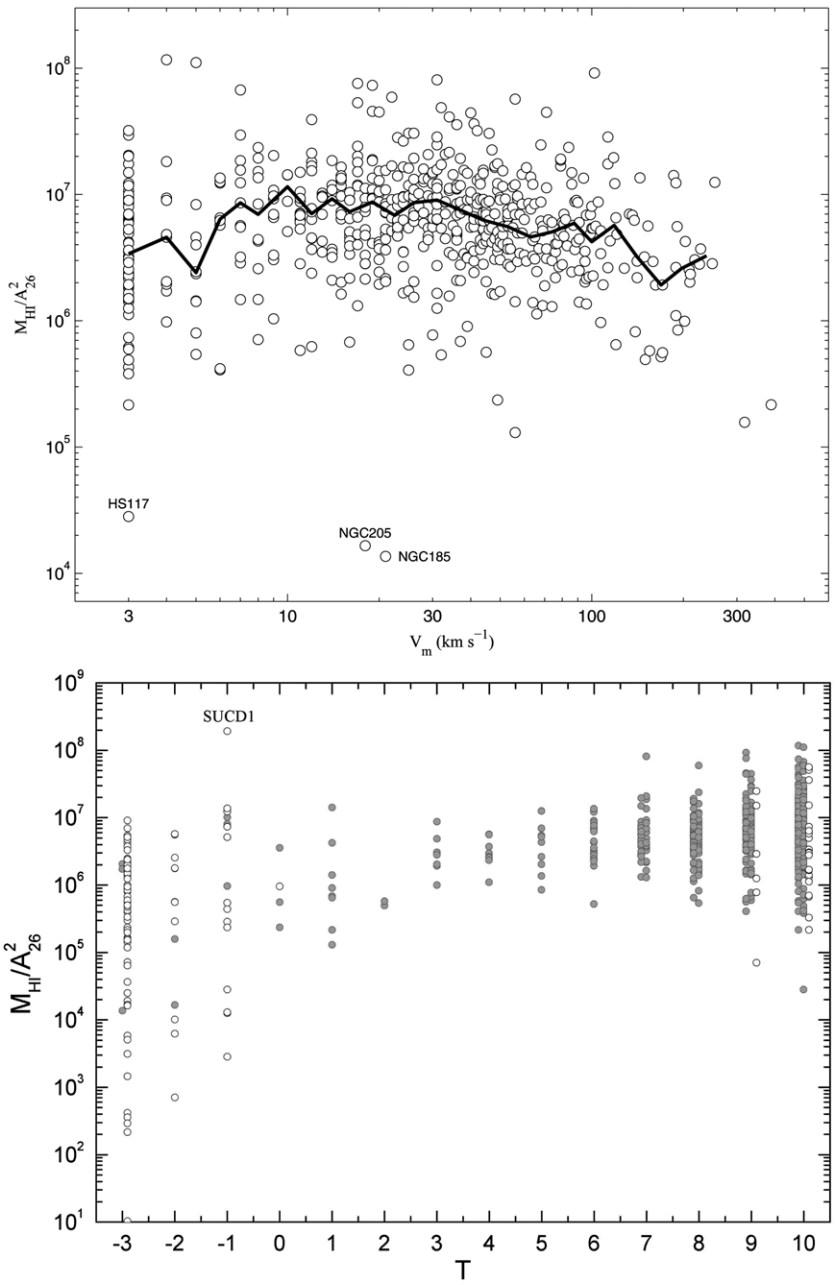

Figure 15. Relation between mean surface density of hydrogen mass and rotation velocity for LV galaxies is shown in the top panel. The thick line represents the running median. The dependence of mean surface density vs. morphological type is presented in the bottom panel. Objects with the upper limit of hydrogen mass are shown by open circles.

$\sim$10 Myr, characteristic for the glow of the most massive stars. Another SFR estimate can be obtained from the integral FUV flux of galaxy, the values of which are presented in Table 1 in the form of $m_{\rm FUV}$ magnitudes. Following Lee et al. (2011), we have used the relation

$$\log(\mathrm{SFR}[M_\odot\,\mathrm{yr}^{-1}]) = 2.78 - 0.4m^c_{\rm FUV} + 2\log D, \qquad (17)$$

where D is in Mpc, and the apparent FUV magnitude is corrected for extinction as

$$m^c_{\rm FUV} = m_{\rm FUV} - 1.93\big(A^G_B + A^i_B\big). \qquad (18)$$

The SFR values from Equations (17) and (18) refer to a characteristic glow time $\sim$100 Myr, i.e., they are more robust. However, they are much more subject to uncertainty due to poorly known internal extinction in galaxies. Distributions of the specific SFR for 715 galaxies on the scales Θ_1, Θ_5, and Θ_j (Figure 18) in general reproduce the previous distributions. Here, similar to the previous figure, the galaxies with the upper limit of SFR are marked by open circles.

Certain arguments in the literature state that galaxies of low and normal surface brightness significantly differ in their evolutionary history. As follows from the data of Figure 19, the specific SFR, measured by the Hα and FUV fluxes, is practically independent of the mean surface brightness of galaxies in the range of about five magnitudes. The SFR decline becomes noticeable only for the extremely low surface brightness galaxies. The relative hydrogen abundance $M_{\rm H\,I}/L_B$

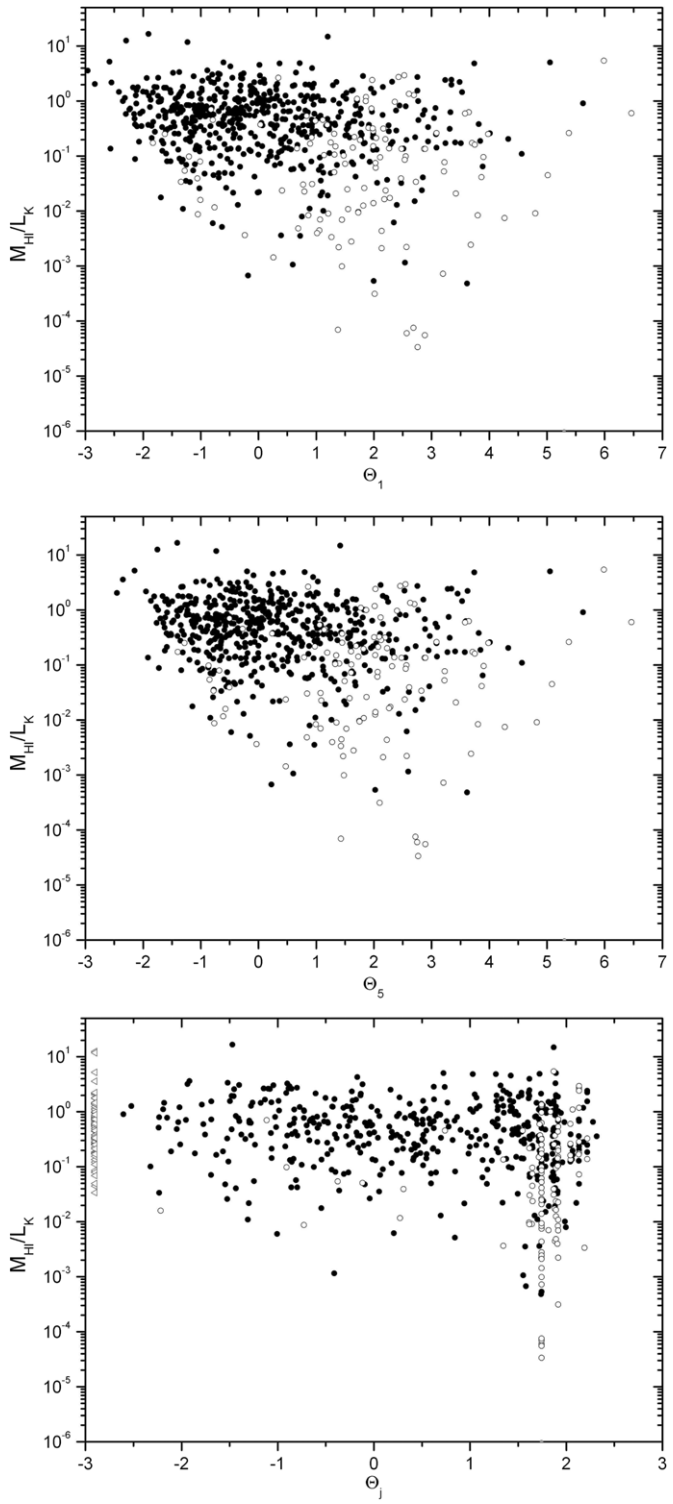

Figure 16. Hydrogen mass-to-*K*-band-luminosity ratio vs. different estimators of the local environment density, i.e., tidal index. Galaxies with a positive tidal index correspond usually to group members. Open circles indicate galaxies with only an upper limit of the H I flux.

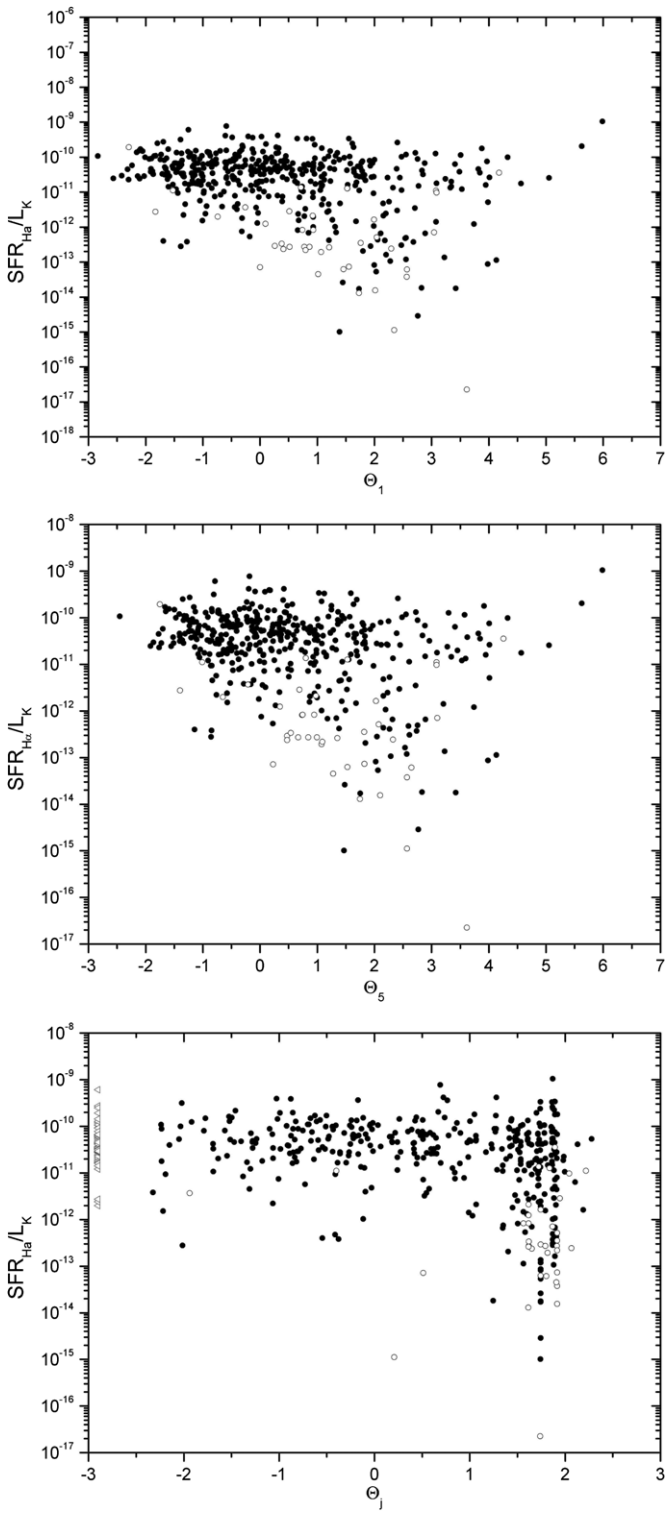

Figure 17. Specific star formation rate for 493 LV galaxies determined from their Hα flux vs. different kinds of tidal index. Galaxies with the upper limit of the Hα flux are indicated by open circles.

grows toward faint surface brightnesses, but at SB $>$ 27 the statistics of the observables becomes poor. These empirical relationships are obviously in need of theoretical interpretation.

9. SOME LOCAL VERSUS GLOBAL PARAMETERS

According to SDSS, the cosmic variation of luminosity in the cubic cell 30 Mpc on a side amounts to $\sim$30% and drops to a value of $\sim$10% in a cell with a side of 95 Mpc (Papai & Szapudi 2010). The local sphere 20 Mpc in diameter contains a number of groups of different populations and morphology, as well as some voids, almost completely devoid of galaxies. It is therefore important to have a quantitative idea of how drastically parameters of the LV differ from the global cosmic parameters.

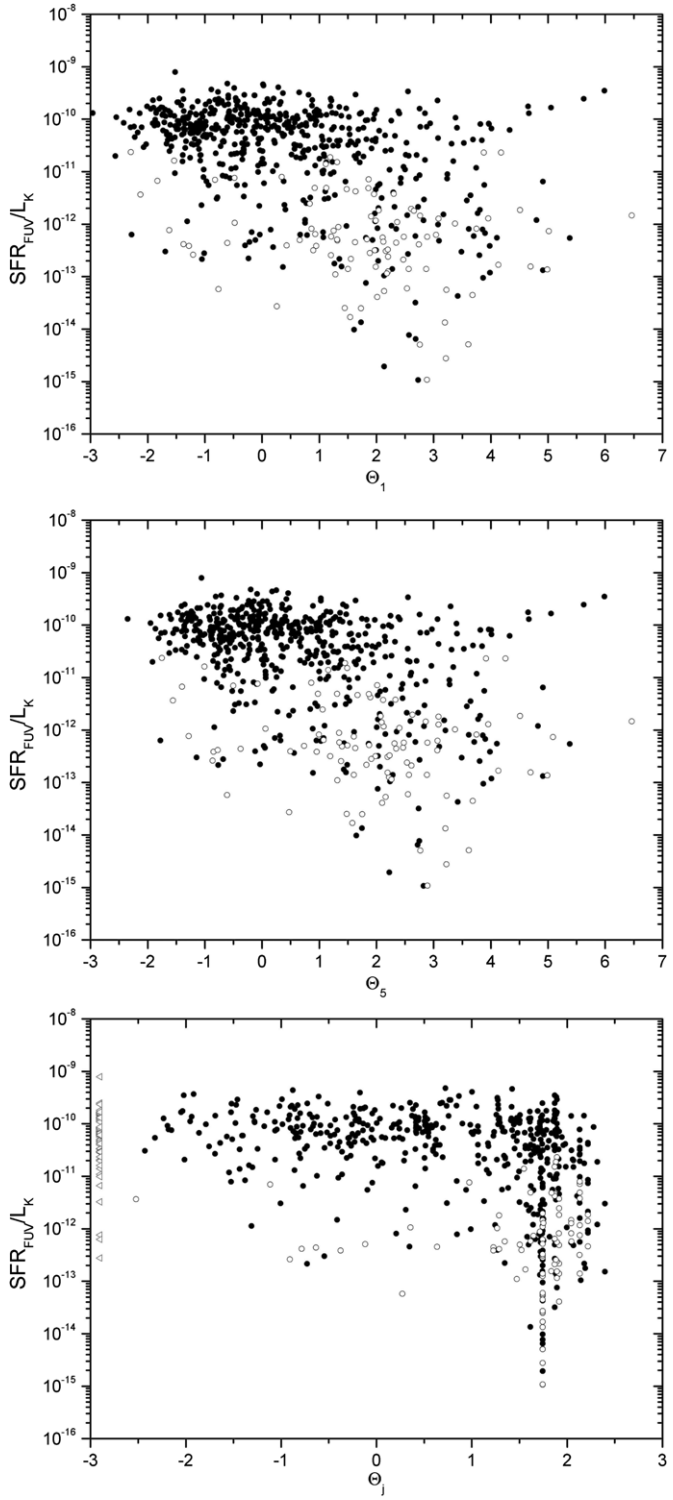

Figure 18. Specific star formation rate for 692 LV galaxies derived from their FUV flux vs. three kinds of tidal index. Open circles indicate galaxies with the upper limit of FUV flux.

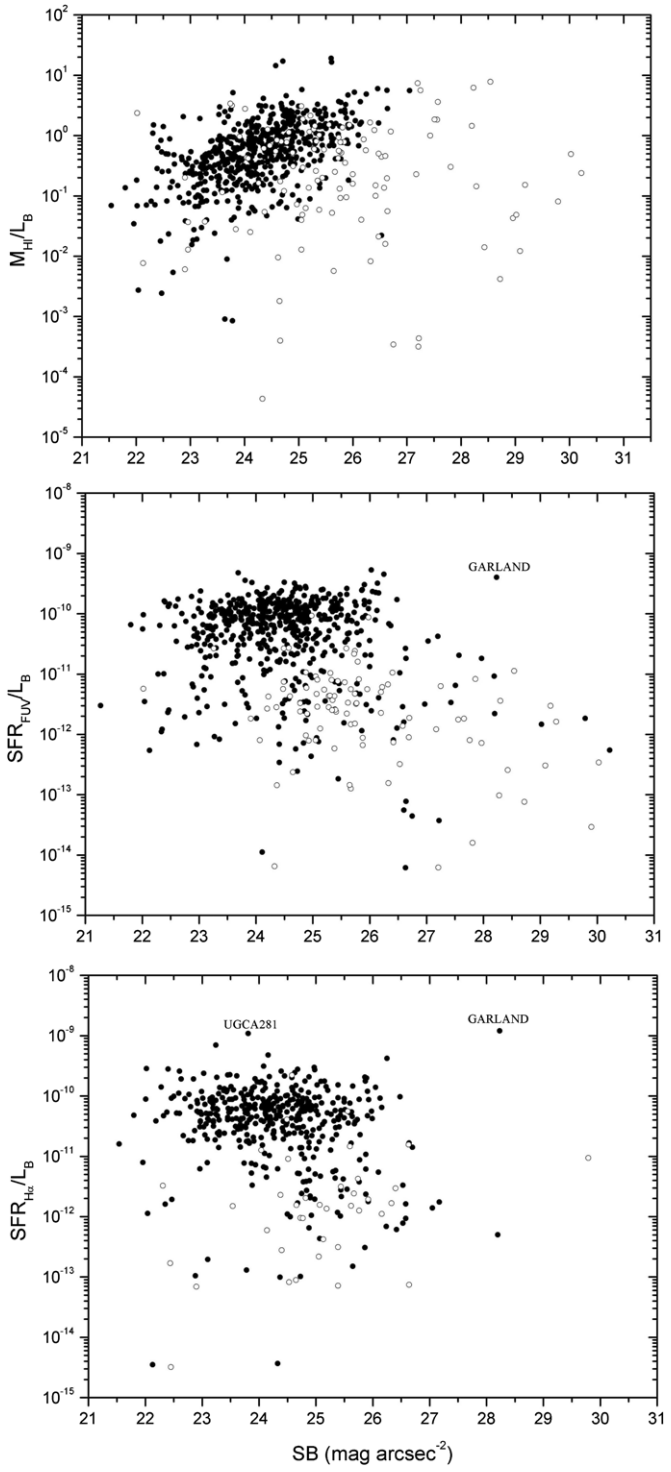

Figure 19. Specific star formation rate and hydrogen mass-to-luminosity ratio in the B band vs. mean surface brightness of the LV galaxies. Open circles indicate galaxies with the upper limit of corresponding fluxes.

The bottom panel of Figure 20 shows the behavior of the average luminosity density in the B band (triangles) and K band (circles) inside spheres of fixed radii. Within a radius of $D = 10$ Mpc the average B-luminosity density $3.0 \times 10^8\ L_\odot\ \mathrm{Mpc}^{-3}$ is 2.2 times higher than its global value $(1.3 \pm 0.1) \times 10^8\ L_\odot\ \mathrm{Mpc}^{-3}$ according to Blanton et al. (2003) and Liske et al. (2003). For the K-luminosity density, the local value $j_K(D < 10\ \mathrm{Mpc}) = 5.9 \times 10^8\ L_\odot\ \mathrm{Mpc}^{-3}$ is just 1.4 times greater than the global one, $4.28 \times 10^8\ L_\odot\ \mathrm{Mpc}^{-3}$ (Jones et al. 2006). Consequently, despite the presence of the Local Void, the LV represents an overdensity of moderate amplitude.

A similar relation between the mean density of hydrogen mass and the radius of the sphere within which it was determined, is shown in the middle panel of Figure 20. The local density $0.54 \times 10^8\ L_\odot\ \mathrm{Mpc}^{-3}$ within $D = 10$ Mpc is close to the

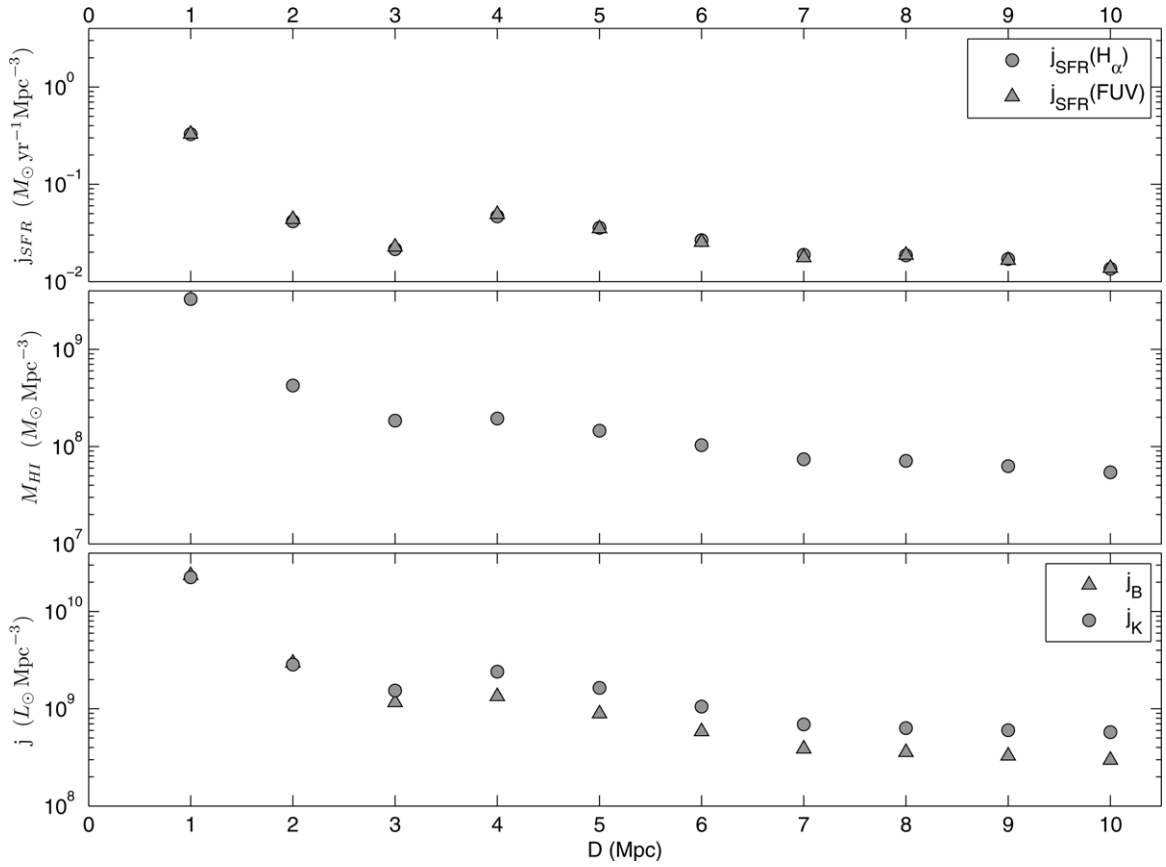

Figure 20. Average density of luminosity in *B* and *K* bands within a distance *D* around our Galaxy (bottom). (Middle) The same for the hydrogen mass density and (Top) for the star formation rate estimated either from Hα fluxes or FUV fluxes.

global mean density of $(0.59 \pm 0.05) \times 10^8\ L_\odot$ Mpc^{-3} according to HIPASS (Zwaan et al. 2003) and ALFALFA (Martin et al. 2010). The top panel of Figure 20 reproduces the variation of the average density of the SFR within a fixed distance *D*. The values of $j_{\rm SFR}$ ($M_\odot$ yr^{-1} Mpc^{-3}), obtained from Hα-fluxes of galaxies, are shown by circles, and the estimates made by FUV fluxes from the *GALEX* are shown by triangles. Agreement between the independent estimates of $j_{\rm SFR}$ can be considered to be quite fair, taking into account the uncertainties related to the corrections for extinction in the FUV band. The mean value from Hα and FUV fluxes within 10 Mpc amounts to $j_{\rm SFR} = (0.014 \pm 0.003)$. Given a certain incompleteness in our Hα survey on the outskirts of the LV, as well as the incompleteness of the UV survey in the region of strong Galactic extinction, this value is consistent with the global average value $(0.018 \pm 0.003)\ M_\odot$ yr^{-1} Mpc^{-3} according to Salim et al. (2007) and James et al. (2008).

Therefore, the sample of galaxies in the LV is quite a suitable representative of the Local universe in plenty of its characteristics. It should be emphasized, however, that only 40% of the galaxies in this sample have distance estimates that are more accurate than (10–15)%. The painstaking observational task of measuring the distances to several hundreds of galaxies within 10 Mpc is a rather pressing issue in the cosmology of the nearby universe. Strictly speaking, the catalog presented here should be called merely a sample of candidate members of the LV.

We thank Valentina Karachentseva and Brent Tully for useful comments and suggestions to improve the text. We are grateful to the anonymous referee for a prompt report that helped us improve the manuscript. This work was supported by the Russian Foundation for Basic Research, grants 10-02-00123, 11-02-00639, 11-02-90449, and RFBR-DFG grant 12-02-91338. We acknowledge the support of the Ministry of Education and Science of the Russian Federation, grant No. 14.740.11.0901 and the project 2012-1.5-12-000-1011-004. Support for proposals GO 12546, 12877, and 12878 was provided by NASA through grants from the Space Telescope Science Institute, which is operated by the Association of Universities for Research in Astronomy, Inc., under NASA contract NAS5-26555. We acknowledge the use of the HyperLeda database (http://leda.univ-lyon1.fr). This research has made use of the NASA/IPAC Extragalactic Database (NED) which is operated by the Jet Propulsion Laboratory, California Institute of Technology, under contract with the National Aeronautics and Space Administration. We also have made extensive use of the following Web services of surveys: the *Galaxy Evolution Explorer* (*GALEX*), the Two Micron All Sky Survey (2MASS), the H I Parkes All Sky Survey (HIPASS), the Arecibo Legacy Fast ALFA Survey (ALFALFA), the Extragalactic Distance Database (EDD), the Sloan Digital Sky Survey (SDSS), the Digitized Sky Surveys (DSS), and the SAO/NASA Astrophysics Data System (ADS).

APPENDIX A

LIST OF APPARENT MAGNITUDES

The compilation of apparent magnitudes of galaxies is presented in Table 3. They are collected from the literature and from surveys and are not corrected for Galactic extinction or for any other effect. The columns contain the following information.

Table 3
List of Apparent Magnitudes

Name	Mag	e_{mag}	Passband	Bibcode	Refs
UGC 12894	17.57	0.10	FUV	2012LV.Magnitude..K	Current work
UGC 12894	16.80		B	2011LV.Magnitude..K	Current work
UGC 12894	19.91	0.08	Ha	2008ApJS..178..247K	Kennicutt et al. 2008
UGC 12894	15.66		H I	2011LV.HI.....K	Current work
WLM	12.80	0.05	FUV	2011ApJS..192....6L	Lee et al. 2011
WLM	11.03		B	1991RC3.9.C...0000d	de Vaucouleurs 1991
WLM	15.56	0.32	Ha	2008ApJS..178..247K	Kennicutt et al. 2008
WLM	9.00	0.50	Ks	2012LV.Magnitude..K	Current work
WLM	11.19		H I	2009ApJ...696..385G	Grcevich et al. 2009

(This table is available in its entirety in machine-readable and Virtual Observatory (VO) forms in the online journal. A portion is shown here for guidance regarding its form and content.)

Table 4
List of Heliocentric Velocities

Name	cz	Error	Bibcode	Refs
UGC 12894	335	22	1992ApJS...81....5S	Schneider et al. 1992
WLM	−122	2	2004AJ....128...16K	Koribalski et al. 2004
And XVIII	−332	3	2012ApJ...752...45T	Tollerud et al. 2012
ESO 409-015	726	18	2005MNRAS.361...34D	Doyle et al. 2005
AGC 748778	258	2	2011AJ....142..170H	Haynes et al. 2011
And XX	−456	3	2012arXiv1211.2638W	Watkins et al. 2012
UGC 00064	305	17	2003A&A...406..829B	Braun et al. 2003
ESO 349-031	221	6	2004AJ....128...16K	Koribalski et al. 2004
NGC 0024	550	18	2005MNRAS.361...34D	Doyle et al. 2005
NGC 0045	465	18	2005MNRAS.361...34D	Doyle et al. 2005

(This table is available in its entirety in machine-readable and Virtual Observatory (VO) forms in the online journal. A portion is shown here for guidance regarding its form and content.)

Table 5
List of Inner Kinematics

Name	w50	Error	Bibcode	Refs
UGC 12894	34		1992ApJS...81....5S	Schneider et al. 1992
WLM	53	18	2004AJ....128...16K	Koribalski et al. 2004
ESO 409-015	53		2005MNRAS.361...34D	Doyle et al. 2005
AGC 748778	16	3	2011AJ....142..170H	Haynes et al. 2011
UGC 00064	60		2003A&A...406..829B	Braun et al. 2003
ESO 349-031	30	18	2004AJ....128...16K	Koribalski et al. 2004
NGC 0024	213		2005MNRAS.361...34D	Doyle et al. 2005
NGC 0045	172		2005MNRAS.361...34D	Doyle et al. 2005
NGC 0055	169	18	2004AJ....128...16K	Koribalski et al. 2004
NGC 0059	50	2	2000A&AS..141..469H	Huchtmeier et al. 2000b

(This table is available in its entirety in machine-readable and Virtual Observatory (VO) forms in the online journal. A portion is shown here for guidance regarding its form and content.)

1. Main name of the galaxy, corresponding to the main name in Table 1.
2. Apparent total magnitude of the galaxy or its lower limit (marked by the symbol "<"). Hα and H I fluxes were transformed to magnitudes using the following equations: $m_{H\alpha} = -2.5\log(F_{H\alpha}) - 13.64$ and $m_{21} = 17.4 - 2.5\log F_{H\,I}$, correspondingly.
3. Measurement error. We estimate the uncertainty of eyeball *B*-band measurements, which were made by our team, to be $\sim 0^m.5$.
4. Photometric passband. We have collected the data for FUV, *B*, Hα, *Ks*, and H I passbands.
5. Bibcode for a measurement. The measurements of our team are marked by bibcode 2011LV.Magnitude..K or 2012LV.Magnitude..K.
6. Reference.

APPENDIX B

LIST OF HELIOCENTRIC VELOCITIES

Table 4 presents the compilation of heliocentric velocities of galaxies. The catalog is organized as follows.

1. Main name of the galaxy, corresponding to the main name in Table 1.
2. Heliocentric velocity (cz) in km s^{-1}.
3. The corresponding error.
4. Bibcode for the measurement.
5. Reference.

APPENDIX C

LIST OF INNER KINEMATIC

The compilation of data on inner kinematics of galaxies is presented in Table 5.

1. Main name of the galaxy, corresponding to the main name in Table 1.
2. Observed H I line width at the 50% level in km s^{-1}.
3. The corresponding error.
4. Bibcode for the measurement.
5. Reference.

APPENDIX D

LIST OF DISTANCES

Table 6 contains the compilation of distances to nearby galaxies.

1. Main name of the galaxy corresponding to the main name in Table 1.
2. Distance modulus.
3. The corresponding error.
4. Method of the estimation. (TRGB)—by the tip of the red giant branch; (Cep)—from the Cepheid luminosity; (SN)—from the supernova luminosity; (SBF)—from galaxy surface brightness fluctuations; (mem)—from galaxy membership in known groups with measured distances of other members; (TF, FP)—by the Tully–Fisher relation or by the fundamental plane; (BS)—by the luminosity of the brightest stars; (CMD)—by the color–magnitude

Table 6
List of Distances

Name	Modulus	Error	Method	Bibcode	Refs
UGC 12894	29.64		TF	2012LV.Distance...K	Current work
WLM	24.93	0.04	TRGB	2007ApJ...661..815R	Rizzi et al. 2007
And XVIII	25.66	0.13	TRGB	2008ApJ...688.1009M	McConnachie et al. 2008
ESO 409-015	29.43		TF	2011LV.Distance...K	Current work
AGC 748778	28.66		h'	2011ApJ...739L..22C	Cannon et al. 2011
And XX	24.52	0.49	TRGB	2008ApJ...688.1009M	McConnachie et al. 2008
UGC 00064	29.91		TF	2011LV.Distance...K	Current work
ESO 349-031	27.53	0.18	TRGB	2006AJ....131.1361K	Karachentsev et al. 2006
NGC 0024	29.98		TF	2011LV.Distance...K	Current work
NGC 0045	29.82		TF	2011LV.Distance...K	Current work

(This table is available in its entirety in machine-readable and Virtual Observatory (VO) forms in the online journal. A portion is shown here for guidance regarding its form and content.)

diagram using some prominent features or simultaneous distance and stellar population fitting; (HB)—by the horizontal branch; (RR)—from the luminosity of RR Lyrae stars; (PNLF)—by the planetary nebula luminosity function; (h, h′)—by the Hubble velocity–distance relation at $H_0 = 73$ km s^{-1} Mpc^{-1}, not accounting for (h) or in view of (h′) a certain Virgocentric flow model; (txt)—by texture of objects indicating their likely proximity.

5. Bibcode for the measurement.
6. Reference.

REFERENCES

Abazajian, K. N., Adelman-McCarthy, J. K., Agueros, M. A., et al. 2009, ApJS, 182, 543
Bell, E. F., McIntosh, D. H., Katz, N., & Weinberg, M. D. 2003, ApJS, 149, 289
Belokurov, V., Zucker, D. B., Evans, N. W., et al. 2006, ApJL, 647, L111
Binney, J., & Merrifield, M. (ed.) 1998, Galactic Astronomy (Princeton, NJ: Princeton Univ. Press)
Blanton, M. R., Hogg, D. W., Brinkmann, J., et al. 2003, ApJ, 592, 819
Braun, R., Thilker, D., & Walterbos, R. A. M. 2003, A&A, 406, 829
Bremnes, T., Binggeli, B., & Prugniel, P. 1998, A&AS, 129, 313
Bremnes, T., Binggeli, B., & Prugniel, P. 1999, A&AS, 137, 337
Bremnes, T., Binggeli, B., & Prugniel, P. 2000, A&AS, 141, 211
Buzzoni, A. 2005, MNRAS, 361, 725
Cannon, J. M., Giovanelli, R., Haynes, M. P., et al. 2011, ApJL, 739, L22
Chiboucas, K., Karachentsev, I. D., & Tully, R. B. 2009, AJ, 137, 3009
Côté, S., Freeman, K., Carignian, C., & Quinn, P. J. 1997, AJ, 114, 1313
Dalcanton, J. J., Williams, B. F., Seth, A. C., et al. 2009, ApJS, 183, 67
de Vaucouleurs, G., de Vaucouleurs, A., Corwin, H., et al. 1991, Third Reference Catalogue of Bright Galaxies (New York: Springer)
Doyle, M. T., Drinkwater, M. J., Rohde, D. J., et al. 2005, MNRAS, 361, 34
Fingerhut, R. L., McCall, M. L., Argote, M., et al. 2010, ApJ, 716, 792
Fouqué, P., & Paturel, G. 1985, A&A, 150, 192
Fukugita, M., & Peebles, P. J. E. 2004, ApJ, 616, 643
Fukugita, M., Shimasaku, K., & Ichikawa, T. 1995, PASP, 107, 945
Gil de Paz, A., Boissier, S., Madore, B. F., et al. 2007, ApJS, 173, 185
Giovanelli, R., Haynes, M. P., Kent, B. R., et al. 2005, AJ, 130, 2598
Grcevich, J., & Putman, M. E. 2009, ApJ, 696, 385
Haynes, M. P., Giovanelli, R., Martin, A. M., et al. 2011, AJ, 142, 170
Huchtmeier, W. K., Karachentsev, I. D., & Karachentseva, V. E. 2001, A&A, 377, 801
Huchtmeier, W. K., Karachentsev, I. D., & Karachentseva, V. E. 2003, A&A, 401, 483
Huchtmeier, W. K., Karachentsev, I. D., Karachentseva, V. E., & Ehle, M. 2000, A&AS, 141, 469
Huchtmeier, W. K., Karachentsev, I. D., Karachentseva, V. E., & Ehle, M. 2000b, A&AS, 141, 469
Ibata, R., Martin, N. F., Irwin, M., et al. 2007, ApJ, 671, 1591
James, P. A., Knapen, J. H., Shane, N. S., et al. 2008, A&A, 482, 507
Jarrett, T. H., Chester, T., Cutri, R., Schneider, S. E., & Huchra, J. P. 2003, AJ, 125, 525
Jarrett, T. N., Chester, T., Cutri, R., et al. 2000, AJ, 119, 2498
Jones, D. H., Peterson, B. A., Colless, M., & Saunders, W. 2006, MNRAS, 369, 25
Kaisin, S. S., & Karachentsev, I. D. 2006, Afz, 49, 337
Kaisin, S. S., & Karachentsev, I. D. 2008, A&A, 479, 603
Kaisina, E. I., Makarov, D. I., Karachentsev, I. D., & Kaisin, S. S. 2012, AstBu, 67, 115
Karachentsev, I. D. 1994, A&AT, 6, 1
Karachentsev, I. D. 2005, AJ, 129, 178
Karachentsev, I. D., & Kaisin, S. S. 2007, AJ, 133, 1883
Karachentsev, I. D., & Kaisin, S. S. 2010, AJ, 140, 1241
Karachentsev, I. D., Karachentseva, V. E., Huchtmeier, W. K., & Makarov, D. I. 2004, AJ, 127, 2031 (CNG)
Karachentsev, I. D., Dolphin, A., Tully, R. B., et al. 2006, AJ, 131, 1361
Karachentsev, I. D., Kashibadze, O. G., Makarov, D. I., & Tully, R. B. 2009, MNRAS, 393, 1265
Karachentsev, I. D., & Makarov, D. I. 1996, AJ, 111, 794
Karachentsev, I. D., & Makarov, D. I. 1999, in IAU Symp. 186, Galaxy Interactions at Low and High Redshift, ed. J. E. Barnes & D. B. Sanders (Cambridge: Cambridge Univ. Press), 109
Karachentsev, I. D., Makarov, D. I., & Huchtmeier, W. K. 1999, A&AS, 139, 97
Karachentsev, I. D., Nasonova, O. G., & Courtois, H. M. 2011, ApJ, 743, 123
Karachentseva, V. E., & Karachentsev, I. D. 1998, A&AS, 127, 409
Karachentseva, V. E., & Karachentsev, I. D. 2000, A&AS, 146, 359
Karachentseva, V. E., Karachentsev, I. D., & Richter, G. M. 1999, A&AS, 135, 221
Kennicutt, R. C. 1998, ARA&A, 36, 189
Kennicutt, R. C., Lee, J. C., Funes, J. G., et al. 2008, ApJS, 178, 247
Kilborn, V. A., Webster, R. L., Staveley-Smith, L., et al. 2002, AJ, 124, 690
Koribalski, B. S., Staveley-Smith, L., Kilborn, V. A., et al. 2004, AJ, 128, 16
Kovaĉ, K., Oosterloo, T. A., & van der Hulst, J. M. 2009, MNRAS, 400, 743
Kraan-Korteweg, R. C. 1986, A&AS, 66, 255
Kraan-Korteweg, R. C., & Tammann, G. A. 1979, AN, 300, 181
Lee, J. C., Gil de Paz, A., Kennicutt, R. C., et al. 2011, ApJS, 192, 6
Lee, M. G., Freedman, W. L., & Madore, B. F. 1993, AJ, 106, 964
Liske, J., Lemon, D. J., Driver, S. P., et al. 2003, MNRAS, 344, 397
Makarova, L. N., Karachentsev, I. D., Rizzi, L., et al. 2009, MNRAS, 397, 1672
Martin, A. M., Papastergis, E., Giovanelli, R., et al. 2010, ApJ, 723, 1359
Martin, D. C., Fanson, J., Schiminovich, D., et al. 2005, ApJL, 619, L1
Martin, N. F., McConnachie, A. W., Irwin, M., et al. 2009, ApJ, 705, 758
Masters, K. L. 2005, PhD thesis, Cornell Univ.
Mathews, L. D., Gallagher, J. S., & Littleton, J. E. 1995, AJ, 110, 581
McConnachie, A. W., Huxor, A., Martin, N. F., et al. 2008, ApJ, 688, 1009
Meyer, M. J., Zwaan, M. A., Webster, R. L., et al. 2004, MNRAS, 350, 1195
Navarro, J. F., Frenk, C. S., & White, S. D. M. 1996, ApJ, 462, 563
Papai, P., & Szapudi, I. 2010, ApJ, 725, 2078
Pasquali, A., Larsen, S., Ferreras, I., et al. 2005, AJ, 129, 148
Paturel, G., Andernach, H., Bottinelli, L., et al. 1997, A&AS, 124, 109
Paturel, G., Petit, C., Prugniel, P., et al. 2003, A&A, 412, 45
Peebles, P. J. E. 1993, Principles of Physical Cosmology (Princeton, NJ: Princeton Univ. Press)
Peebles, P. J. E., & Nusser, A. 2010, Natur, 465, 565
Peebles, P. J. E., Phelps, S. D., Shaya, E. J., & Tully, R. B. 2001, ApJ, 554, 104
Rizzi, L., Tully, R. B., Makarov, D. I., et al. 2007, ApJ, 661, 815
Roberts, M. S., & Haynes, M. P. 1994, ARA&A, 32, 115

Salim, S., Rich, R. M., Charlot, S., et al. 2007, ApJS, 173, 267
Sandage, A., & Tammann, G. A. 1981, Revised Shapley-Ames Catalog of Bright Galaxies (Washington, DC: Carnegie Institution), 635
Schlegel, D. J., Finkbeiner, D. P., & Davis, M. 1998, ApJ, 500, 525
Schneider, S. E., Thuan, T. X., Mangum, J. G., & Miller, J. 1992, ApJS, 81, 5
Spergel, D. N., Bean, R., Doré, O., et al. 2007, ApJS, 170, 377
Staveley-Smith, L., Juraszek, S., Koribalski, B. S., et al. 1998, AJ, 116, 2717
Tollerud, E. J., Beaton, R. L., Geha, M. C., et al. 2012, ApJ, 752, 45
Tonry, J. L., Stubbs, C. W., Lykke, K. R., et al. 2012, ApJ, 750, 99
Tully, R. B. 1988, Nearby Galaxies Catalog (Cambridge: Cambridge Univ. Press)
Tully, R. B., & Fouqué, P. 1985, ApJS, 58, 67
Tully, R. B., Shaya, E. J., Karachentsev, I. D., et al. 2008, ApJ, 676, 184
Vaduvescu, O., McCall, M. L., Richer, M. G., & Fingerhut, R. L. 2005, AJ, 130, 1593
Vaduvescu, O., Richer, M. G., & McCall, M. L. 2006, AJ, 131, 1318
Verheijen, M. A. W. 2001, ApJ, 563, 694
Watkins, L. L., Wyn Evans, N., & van de Ven, G 2012, arXiv:1211.2638
Weisz, D. R., Dalcanton, J. J., Williams, B. F., et al. 2011, ApJ, 739, 5
Willman, B., Dalcanton, J. J., Martinez-Delgado, D., et al. 2005, ApJL, 626, L85
Wong, O. I., Ryan-Weber, E. V., Garcia-Appadoo, D. A., et al. 2006, MNRAS, 371, 1855
Zwaan, M. A., Staveley-Smith, L., Koribalski, B. S., et al. 2003, AJ, 125, 2842